Article:
Li, X, Jaworski, AJ and Mao, X orcid.org/0000-0002-9004-2081 (2018) Comparative study of two non-intrusive measurement methods for bubbling gas-solids fluidized beds: electrical capacitance tomography and pressure fluctuations. Flow Measurement and Instrumentation, 62. pp. 255-268. ISSN 0955-5986

https://doi.org/10.1016/j.flowmeasinst.2017.08.002

Comparative study of two non-intrusive measurement methods for bubbling gas-solids fluidized beds: electrical capacitance tomography and pressure fluctuations

Xiaoxu Li, Artur J. Jaworski, Xiaoan Mao

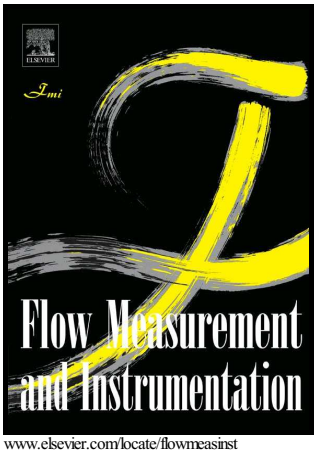

www.elsevier.com/locate/flowmeasinst

PII: S0955-5986(17)30209-1
DOI: http://dx.doi.org/10.1016/j.flowmeasinst.2017.08.002
Reference: JFMI1341

To appear in: *Flow Measurement and Instrumentation*

Received date: 8 May 2017
Revised date: 1 July 2017
Accepted date: 9 August 2017

Cite this article as: Xiaoxu Li, Artur J. Jaworski and Xiaoan Mao, Comparative study of two non-intrusive measurement methods for bubbling gas-solids fluidized beds: electrical capacitance tomography and pressure fluctuations, *Flow Measurement and Instrumentation,* http://dx.doi.org/10.1016/j.flowmeasinst.2017.08.002

Comparative study of two non-intrusive measurement methods for bubbling gas-solids fluidized beds: electrical capacitance tomography and pressure fluctuations

Xiaoxu Li, Artur J. Jaworski* and Xiaoan Mao

Faculty of Engineering, University of Leeds, Woodhouse Lane,
Leeds LS2 9JT, United Kingdom

*Corresponding author: a.j.jaworski@leeds.ac.uk

Abstract

Conventional measurement techniques used to investigate the internal fluid flow processes in gas-solids fluidized beds are known to introduce disturbances to the flow. Two non-intrusive methods: pressure fluctuation measurement and electrical capacitance tomography (ECT) techniques have been usually used separately to study the complex two phase flow phenomena in fluidized beds. However, no systematic study has been carried out to compare these two methods in terms of their capabilities to reveal the hydrodynamic characteristics of fluidized beds. This paper presents a comparative study between these two non-intrusive measurement techniques within a bench-scale fluidized bed. Experiments were carried out using two alternative test sections (one equipped with pressure transducers, one with ECT sensor) for the same operating conditions. The performance of these two methods was evaluated against some important hydrodynamic parameters within fluidized beds, such as the determination of the minimum fluidization velocity, the determination of the minimum slugging velocity, dominant frequency and bubble rise velocity. The results demonstrate that the two measurement techniques can both provide broadly consistent results, although ECT tends to be more reliable with respect to estimating bubble rise velocity.

Keywords: Fluidized beds, Hydrodynamics, Electrical capacitance tomography, Pressure fluctuations, Non-intrusive methods

1. Introduction

Gas-solids fluidized beds have been widely used in both traditional and modern industrial applications, especially in the areas of chemical engineering, energy conversion, recovery of valuable materials from waste streams and biomass gasification (Sasic et al., 2007; Rautenbach et al., 2013). Undoubtedly, the excellent mixing and an attractive high heat and mass transfer rate between gas and solids phases are attributed to their popularity in industrial applications (Qiu et al., 2014). Therefore, for the purpose of safe operation, reliable scale-up and plant troubleshooting, it is vital to understand the internal performance of the beds with the highest possible degree of accuracy, which, in turn, brings considerable challenges to the implementation of reliable measurement techniques (Makkawi and Wright, 2004).

Numerous conventional measurement techniques have been tried out to investigate the properties of fluidized bed behaviour. Intrusive pressure probes were used to determine the bubble rise velocity in a 15 inch diameter column. The opening sides of all five sets of probes were positioned in the centre of the bed (Chan et al., 1987). Two types of fibre optic probes, forward light scattering and backscattering, were applied by many researchers to investigate the bed and bubble behaviour in terms of the local movement of solid particles, particle concentration, bubble frequency, bubble rise velocity and bubble size distribution, to name but a few (Oki et al., 1975; Rüdisüli et al., 2012; Mainland and Welty, 1995). A parallel plate capacitor probe was applied to study the uniformity of fluidization with a bed of fine particles (Morse and Ballou, 1951). Optimized needle type capacitor probes were employed to derive bubble characteristics, for example, bubble size (pierced length) and bubble rise velocity (Werther, 1974). However, despite the achievements that the above mentioned probes can bring about in studying gas-solids fluidized beds, it is recognized by many researchers that the disturbances and interference introduced by the probes cannot be avoided completely (Rowe and Masson, 1980; Dyakowski et al., 2000).

The current comparative study involves two non-intrusive measurement techniques. The first one, electrical capacitance tomography (ECT), can provide qualitative and quantitative data in monitoring a multi-phase fluid flow system by measuring the electrical capacitances between sets of electrodes placed around a process vessel (Dyakowski et al., 2000). ECT has the advantage of being simple to construct, fast in measurement speed, of low cost and able to withstand harsh operating conditions, i.e. high temperatures and pressures. The second non-intrusive method relies on pressure fluctuation measurements through small diameter and short pressure tappings which lead to the

pressure sensing elements inside the pressure transducers. Therefore there is no pressure probe protruding into the bed. The sensors typically used in the pressure measurements, are robust and relatively cheap (Sasic et al., 2007). The resulting measurements are recorded with an adequately high frequency, enabling the collection of a large amount of information about the internal fluid dynamics of the fluidized bed.

2. Literature Review

As one of the most attractive tomography measurement techniques, ECT has been used by many researchers to study the gas-solids fluidized beds in the bubbling regime, in particular in terms of the bed behaviour and bubble characteristics (Makkawi and Wright, 2002; Du et al., 2005; Wang et al., 1995; Qiu et al., 2014; Wang, 1998). Bed behaviour just above an air distributor was initially observed by Wang et al. (1995) and Wang (1998). In addition, three flow regimes were identified by means of the cross-sectional solids concentration distribution as a function of time. More flow regimes, such as single bubble, slugging bed, turbulent flow and fast fluidization regime, have been then classified by means of ECT measurements in a conventional gas-solids fluidized bed.

The main parameters used in characterizing flow regimes are solid fraction profile, average solid fraction and its standard deviation and dominant frequency of the power spectral density (PSD) function (Makkawi and Wright, 2002). Also, the standard deviation of solids concentration was found to peak at the transition velocity from bubbling to turbulent regime in a 0.3 m diameter bed (Du et al., 2005). Numerous studies have also been focused on the factors influencing the transition velocities. For example, the effect of the ratio of the static bed height to the bed diameter on the transition velocity to turbulent regime was studied by Qiu et al. (2014). However, very few studies were conducted to determine the minimum fluidization velocity and the minimum slugging velocity.

With respect to bubble characteristics within bubbling regime, a great deal of interesting features have been revealed by virtue of the ECT measurements. A method of deriving bubble length within bubbling regime via real time ECT measurements was reported by Wang et al. (1995). Bubble rise velocity has been estimated by means of a twin-plane ECT sensor (Makkawi and Wright, 2004). Bubble diameter was studied by several researchers, although some debate still exists regarding the choice of criterion defining the bubble boundary (Halow et al., 1993; Chandrasekera et al., 2015; Li

et al., 2016). Dominant frequencies from PSD function were used to characterize the bubble frequency (Makkawi and Wright, 2002).

Meanwhile, non-intrusive pressure fluctuation measurements have also been extensively used to identify a wide-range of bed behaviour and bubble characteristics within bubbling regime (Johnsson et al., 2000; Sasic et al., 2007; Wilkinson, 1995). The minimum fluidization velocity can be estimated either by means of the pressure drop or the standard deviation of the pressure fluctuations (Wilkinson, 1995; Svoboda and Hartman, 1981). The latter method was reported to have been able to avoid the need to de-fluidize the bed by decreasing the gas superficial velocity from a vigorous fluidization state when trying to measure the minimum fluidization velocity. Hence, this approach would be much more useful and effective in industrial applications where continuous operations are preferable on account of the financial cost and efficiency of operations. In addition, the standard deviation of the pressure fluctuations has often been utilized to determine the transition velocity, usually denoted by U_c, from bubbling to turbulent regime (van Ommen et al., 2011). Here the transition is marked by the maximum value of the standard deviation. Some researchers pointed out that the transition velocity was influenced by many factors including measuring locations and bed geometries when testing Group A and Group B particles (Bai et al., 1996). However, very few studies involved with identifying the minimum slugging velocity. Qiu et al. (2014) provide a plot of standard deviation of pressure fluctuations versus various gas superficial velocity values. It is possible to infer that the minimum slugging velocity can be determined from the graph. However, the authors have not made this point clear.

Concerning the bubble characteristics within bubbling regime, pressure fluctuations measured at plenum location were used to identify related frequencies within fluidized beds using Fast Fourier Transform (FFT) analysis (Kage et al., 2000). Three peak frequencies derived from the modified PSD function were confirmed to be consistent with the bubble eruption frequency at the freeboard, the bubble generation frequency above gas distributor and the spontaneous frequency of the fluidized bed. It was reported that bubble rise velocities were obtained from different pairs of pressure taps by means of cross-correlation function (Fan et al., 1983). However, the origin of the derived velocities has not been fully discussed and also the obtained results have not been validated with empirical correlations.

Very few studies have been conducted to compare the performance of these two non-intrusive measurement techniques in revealing the complex fluid flow processes. For example, Qiu et al. (2014) carried out experiments choosing different measuring locations and different sampling rates

(60 frames per second for ECT and 170 samples per second for pressure acquisition). In addition, some critical parameters such as the minimum fluidization velocity and the minimum slugging velocity have not been dealt with.

The objective of this paper is to compare and evaluate the performance of two non-intrusive measurement techniques: electrical capacitance tomography (ECT) and pressure fluctuation measurement (using small pressure tappings in the bed wall connected to pressure transducers), within a bench-scale gas-solids fluidized bed in terms of characterising the bed hydrodynamic behaviour. It is hoped that this will allow researchers to make more informed choices when it comes to choosing the suitable non-intrusive measurement techniques. More specifically, different approaches for estimating minimum fluidization velocity and minimum slugging velocity from these two methods are compared and assessed. Similarly, dominant frequency obtained from the PSD function and bubble rise velocity estimated from these two methods are obtained and evaluated in a detail.

3. Experimental

Experimental set-ups for both ECT and pressure fluctuation measurements will be dealt with in this section. The description of experimental set-up for ECT measurement includes the description of the bench-scale fluidized together with the details of the employed ECT system. For the experimental set-up for pressure fluctuations, pressure transducers' specifications, pressure transducer holder design and fabrication and the data acquisition system will be given accordingly.

3.1 Experimental set-up for ECT measurement

The schematic diagram for ECT experimental rig is presented on the left of **Fig. 1**. The fluidizing medium is air at atmospheric pressure, provided from a compressed air cylinder (1). A needle valve (2) acts as the isolation valve and controls the air flowing into the fluidized bed. Gas flow rate was obtained via a float type flow meter (3) before the air was introduced into the bed. The corresponding gas superficial velocity was acquired from the gas flow rate divided by the cross-sectional area. The bench-scale gas-solids fluidized bed comprises a 59 mm internal diameter (3 mm wall thickness) acrylic pipe with the length of 1 meter which forms the fluidized bed vessel (7). Use of transparent material allows visual observation to assist preliminary qualitative analysis.

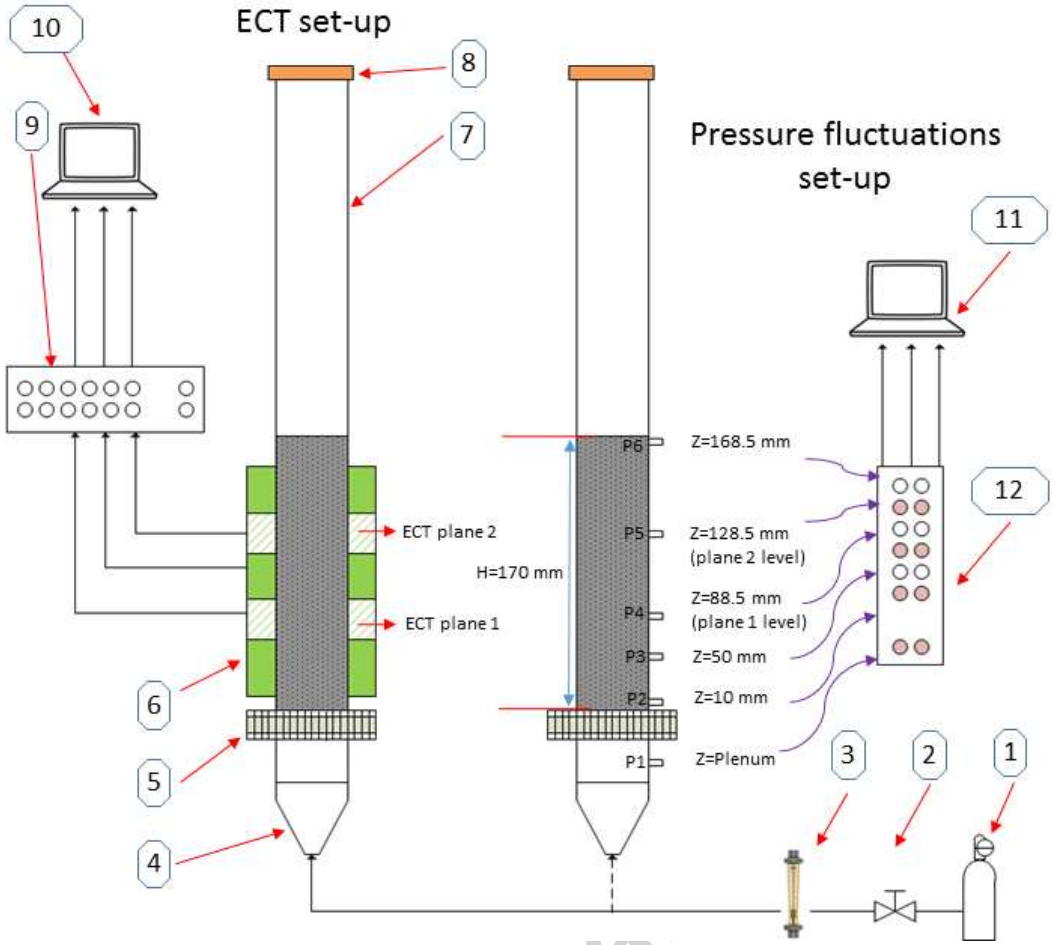

Fig. 1. Schematic diagram of experimental setups. 1 – Compressed air cylinder; 2 – Needle valve; 3 – Float flowmeter; 4 – Plenum; 5 – Air distributor; 6 – Twin-plane ECT sensor; 7 – Fluidized bed vessel; 8 – Top-end cap. For ECT setup shown on the left: 9 – Capacitance measurement unit; 10 – Host PC for ECT. For pressure measurement setup shown on the right: 11 – Host PC for pressure fluctuations; 12 – DAQ data acquisition card; symbols P1 – P6 refer to locations of pressure transducers.

A perforated PVC distributor (5) was designed and sandwiched by flanges between the bed pipe (7) and the air plenum (4) to make the upward air flow uniform. The distributor has 48 holes of 1 mm diameter giving the total area of the holes in the distributor of 3.768 x 10-5 m^2 (1.38% of the total effective area). A piece of fine mesh was placed on top of the air distributor to prevent any particles from falling down into the plenum. Silica sand was used as granular material. The density of silica sand is 2650 kg/m^3, and its mean diameter is 276 microns, i.e. it belongs to the Geldard classification of Group B particles for fluidization (Geldart, 1973). In order to prevent the solids from blowing out of the bed, a customized cap (8) with an embedded fine mesh disk was mounted on top of the bed pipe. The static height of the fluidized bed is kept at 170 mm, which ensures that the granular material completely covers the ECT sensor electrodes (including guard electrodes) to

keep the electrostatic field as two-dimensional as possible for the configuration calibration (Li et al., 2016).

The ECT measurement system used in the present study is PTL300E made by Process Tomography, Ltd., Cheshire, UK. The main hardware component is the capacitance measurement unit (CMU) which can provide the tomographic measurement rate of up to 200 frames per second (fps) and can measure inter-electrode capacitances in the range of 0.1 to 2000 fF. The tasks of image reconstruction and display are mainly executed by the PTL ECT32v2 software. This is a comprehensive suite of programs enabling the PTL300E system to be configured, calibrated, and utilized to record inter-electrode capacitance data files and to reconstruct them into image files at user-defined speeds (Process Tomography Limited, 2001). The ECT32v2 software was installed on the host PC running Microsoft windows XP. The customized twin-plane ECT sensor (6) can slide over the pipe (7). It has 8 measuring electrodes for each plane (plane 1 is referred to as the lower plane) and the axial length of each measuring electrode is 10 mm. Guard electrodes and external shielding electrodes are provided. The centre to centre distance between two measuring electrode planes is 40 mm.

3.2 Experimental set-up for pressure fluctuation measurement

To enable a comparative study between ECT and pressure fluctuation measurements a replica of the pipe forming the vessel of the bench-scale fluidized bed was built and was equipped with suitable pressure transducer "holders" to facilitate the measurement through small tappings on the inside of the pipe. The replica pipe is shown schematically on the right of **Fig. 1**. Three types of gauge pressure transducers, namely, PX72-0.3GV, PX72-0.8GV, PX72-1.5GV, from Omega Engineering Limited, Manchester, UK, were selected to measure the pressure fluctuations at different locations as shown in **Fig. 1**. The measurement ranges for these three types pressure transducers are 0 – 0.3 psi (2068 Pa), 0 – 0.8 psi (5516 Pa) and 0 – 1.5 psi (10342 Pa), respectively. Pressure transducers with a wider measurement range are placed at positions at the bottom of the bed to cope with higher pressure ranges in this region. All the pressure transducers were calibrated against a U-tube water monometer prior to data acquisition. The linearity and repeatability of the pressure measurements are ±0.5% and ±0.3% of the full span, respectively.

The recorded pressure fluctuation data were collected at a sampling rate of 200 Hz by a DAQ card (DaqTemp Model 14A). Since some crucial frequencies, for example, bubble generation frequency

and bubble burst frequency within fluidized beds, are typically below 10 Hz (Sasic et al., 2007), the choice of 200 Hz for pressure fluctuation measurement would be sufficient to disclose internal flow information. On the other hand, the equivalent 200 Hz sampling rate was chosen to be comparable to the ECT image capture rate of 200 fps (or 200 Hz). The length of collected measurement samples was equivalent to 80 seconds for both measurement methods which was found sufficient for all spectral/correlation analyses.

Figure 2 shows the schematic diagram of a pressure transducer "holder" used in the rig. The pressure transducer is placed inside an M12 bolt (shown in dark grey), which is suitably modified to fit the external shape of the pressure transducer. The transducer is bonded to the bolt using a small amount of silicone sealant. The tip of the bolt is machined to support a small o-ring that provides a seal between the fluidized bed and atmospheric conditions on the outside. The modified bolt is screwed into an acrylic boss which is in turn glued to the wall of the pipe. A small mesh disk is clamped between the modified bolt and the inside of the acrylic boss to keep dust away from the pressure sensor element. The transducer pressure port (shown as a thin-walled pipe in light grey) is aligned with a pressure tapping drilled through the bottom of the acrylic boss and pipe wall. The internal diameter of the pressure tapping is 2.6 mm to match the internal diameter of the pressure port in the transducer body. Normally, the pressure tapping diameter is in the range between 2 and 5 mm. Smaller size will result in signal damping while much larger diameters will increase resonance effects and introduce disturbance to the internal local hydrodynamics (van Ommen et al., 2011). In the present study, 2.6 mm was chosen to ensure all the three parts had a consistent size for the pressure signal to propagate. Pressure fluctuations were measured simultaneously via six pressure transducers which were distributed axially along the bed pipe, as presented in **Fig. 1**. It is worth noting that P4 and P5 are located to coincide with the centre of ECT electrode planes. The operating conditions for both ECT and pressure fluctuation measurements are summarized in **Table.1**.

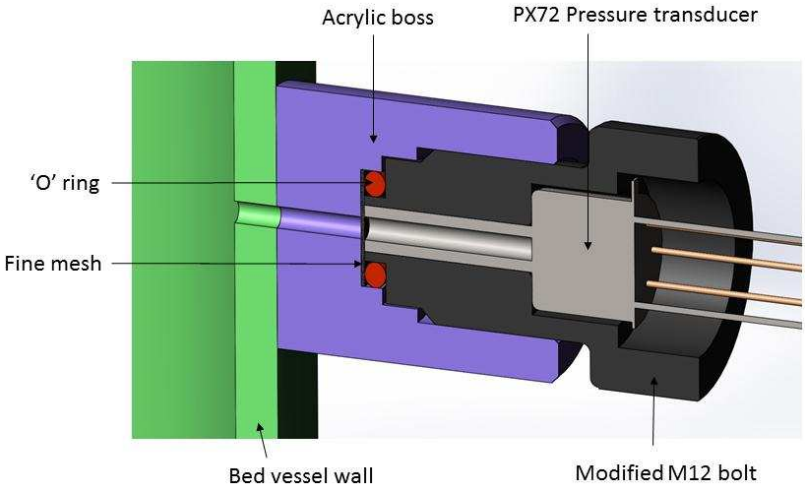

Fig. 2: Schematic drawing of pressure transducer ‘‘holder’’ design.

Table 1 Comparison of measurement methods.

Parameters	ECT	Pressure fluctuations
Sampling rate and duration	200 fps, 80 seconds	200 Hz, 80 seconds
Measuring locations	Plane 1 and plane 2 levels	Six axial measurement levels
Sensors or transducers	Twin plane ECT sensor, eight measuring electrodes (10 mm long) per plane	PX72-0.3GV, PX72-0.8GV and PX72-1.5GV gauge pressure transducers

4. Results and discussion

There are four parameters in total investigated for both non-intrusive methods. The first two are focused on the transition velocities, namely, minimum fluidization velocity and minimum slugging velocity. Another two key parameters are the dominant frequency derived from the PSD function, and the bubble rise velocity derived within bubbling regime.

4.1. Estimation of the minimum fluidization velocity, U_{mf}

As reviewed earlier (Svoboda and Hartman, 1981), the conventional method of deriving U_{mf} relies on measurements of pressure drop across the bed, which is regarded as the simplest and most reliable approach. In the current work, it is used as a benchmark for comparisons with alternative methods outlined below. The estimation of the minimum fluidization velocity using the pressure

drop method is illustrated in **Fig. 3**. Here, the pressure drop (obtained from the time averaged pressure fluctuation signals) is plotted against the decreasing gas superficial velocity. It is worth noting that generally, fluidized beds with Group B particles undergo direct transition between "fixed" and "bubbling" regime (Yang, 2003), and so in effect minimum fluidization velocity is identical with minimum bubbling velocity. Hence, the intersection point of the two curves fitted for "fixed bed" and "bubbling bed" regimes is regarded as the onset of minimum fluidization. **Figure 3** was obtained for six locations presented in **Fig. 1**. It can be seen that the pressure drop shows a logical pressure drop gradient along the bed height where lower height has higher pressure drop due to a thicker layer of gas-solids mixture above the measurement point. The minimum fluidization velocities obtained for the six locations are in good agreement with each other, with the average of 5.56 cm/s. The derived minimum fluidization velocity from the pressure measurement at plenum position, typically used in practical applications for convenience, is 5.62 cm/s which means there is only 1.1% discrepancy between the two values of U_{mf}.

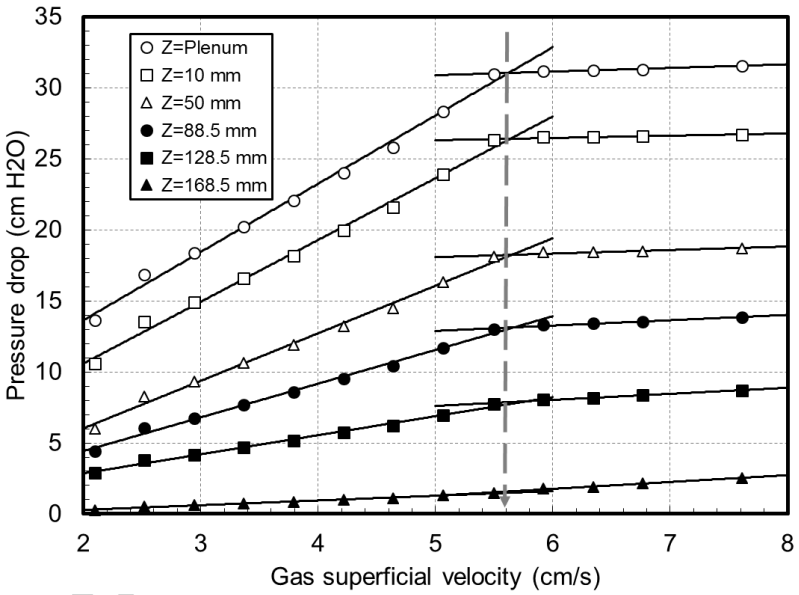

Fig. 3: Pressure drop against gas superficial velocity for different transducer locations.

An alternative method of establishing U_{mf}, used in this work, relies on the analysis of the pressure fluctuations (rather than pressure drop). **Figure 4** illustrates the values of standard deviation of pressure fluctuations at the six different locations plotted against various gas superficial velocities. The dependence of the standard deviation on superficial velocity is such that two straight lines can be fitted (for each pressure tapping position) that correspond to the state of the bed before and after the onset of bubbling regime, respectively. Their intersection seems to indicate a range between about 5 and 5.5 cm/s (note green triangular symbols) that broadly coincides with the values of U_{mf}.

It is interesting to note that some existing publications, notably by Wilkinson (1995) and Johnsson et al. (2000), identify the values of U_{mf} as the intersection points between the X-axis and lines fitted for the bubbling regime. However, the present experimental results, would not allow a direct application of this estimation method since the obtained U_{mf} would be significantly underestimated. For example, the intersection points between the X-axis and fitted lines under bubbling regime would be mostly less than 4 cm/s, giving a very high percent error of 27.8% compared with the value of 5.56 cm/s estimated using the pressure drop approach. Therefore, in the present study the intersection points between two fitted lines (the almost flat line for the fixed bed and sloping line under bubbling regime) are taken as the estimated values of U_{mf}. The reason behind this may be explained by the possibility that the pressure fluctuation data under the fixed bed state must be taken into account when identifying the minimum fluidization velocity. It is possible that initial fluidization must be preceded by the growth of unsteadiness in the gas-solids interactions. All the six intersection points are highlighted by pattern-filled triangular symbols between two dashed arrows indicating the range. Accordingly, the calculated minimum fluidization velocity from these six different heights above the gas distributor are 5.03 cm/s, 5.11 cm/s, 5.37 cm/s, 5.39 cm/s, 5.49 cm/s and 5.0 cm/s, respectively. The corresponding averaged value is 5.23 cm/s. These values are relatively close to values obtained from the pressure drop approach.

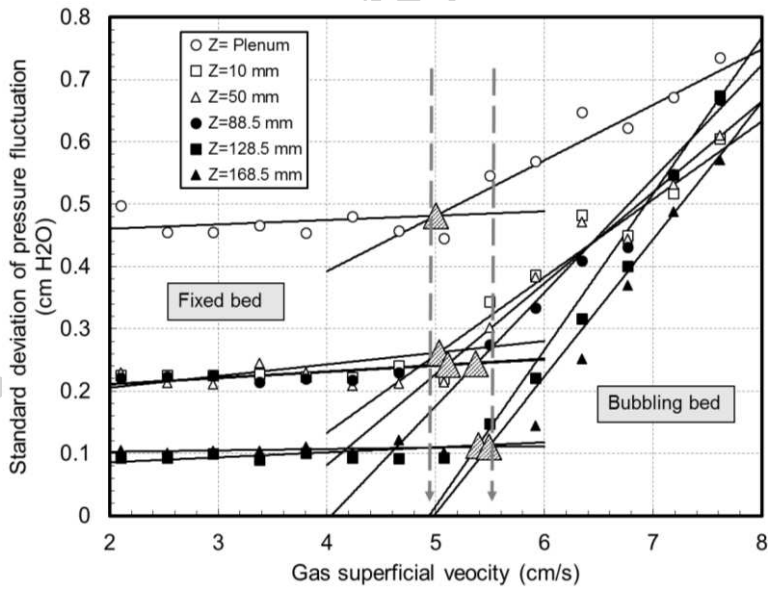

Fig. 4: Standard deviation of pressure fluctuations at different transducer locations.

The second alternative method of estimating U_{mf} considered in this paper relies on analysing the time series data captured via the ECT system. Here, the variable of interest is the temporal variation of the cross-section averaged solids volume fraction, and it is analysed by calculating the standard

deviation of the "signal" defined in this way. The plots of standard deviation of the cross-section averaged volume fraction measured at plane 1 and plane 2 versus gas superficial velocity are presented in **Fig. 5**. The applicability of using ECT data to predict the minimum fluidization velocity has been previously demonstrated by Makkawi and Wright (2002). U_{mf} was defined as the superficial gas velocity at which the bed starts to change from a fixed bed to a bubbling bed when increasing gas flow rate, or in other words the velocity at which the standard deviation equals zero. For the data shown if **Fig. 5** such condition can be obtained from the intersection of the linear fit of the standard deviation data with the X-axis. Theoretically, the two points derived from two different ECT measuring planes should coincide. However, in practice two points, remarkably close to each other, are produced with the corresponding minimum fluidization velocities of 5.22 cm/s and 5.27 cm/s, giving an averaged value of 5.25 cm/s. It is worth noting that this is in line with the results obtained from the pressure drop approach (5.56 cm/s) and standard deviation of pressure fluctuation approach (5.23 cm/s), respectively.

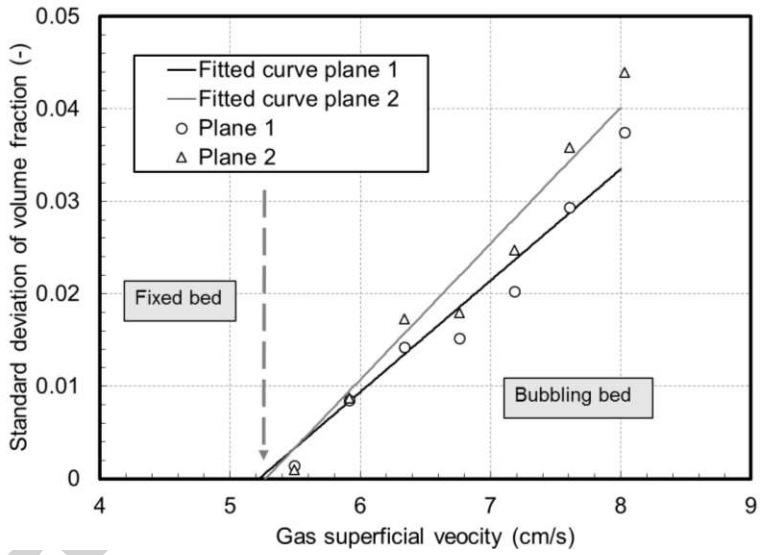

Fig. 5: Standard deviation of cross-section averaged volume fraction measured at two ECT planes.

Finally, it is also possible to evaluate U_{mf} via well-established empirical correlations. The equation proposed by Wen and Yu (1966) has been recognized as one of most extensively accepted empirical correlations for estimating the U_{mf}:

$$(N_{Re})_{mf} = \sqrt{(33.7)^2 + 0.0408 N_{Ga}} - 33.7 \qquad (1)$$

where $(N_{Re})_{mf} = d_p \rho_f U/\mu$ is the particle Reynolds number at the onset of fluidization; $N_{Ga} = {d_p}^3 \rho_f(\rho_s - \rho_f)g/\mu^2$ is Galileo (or Archimedes) number; d_p is the particle diameter; g is acceleration; ρ_s is particle density; ρ_f is fluid density; μ is fluid viscosity; and U is the superficial fluid velocity. The correlation has been established using 284 experimental conditions collected across 14 independent experimental investigations (cf. Fig. 4 in Wen and Yu, 1966). According to the empirical correlation, the diameter of solid particles is one of most sensitive parameters in equation (1). Also, such correlations are strictly speaking derived for mono-dispersed particles, but are typically used for estimations carried out for poly-dispersed particles when the size band is relatively narrow. In order to carry out the estimations of U_{mf} the mean diameter of 276 μm (value obtained from MasterSizer measurement) was used with an added ±10% "error band". Subsequently, the calculated values of U_{mf} range from 4.83 cm/s to 7.19 cm/s.

The results obtained in this section are summarized in **Table 2**. It can be observed that all U_{mf} values obtained from the three experimental approaches are in close agreement with each other. It can also be shown that the predicted range of expected fluidization velocities using the empirical correlation (1) covers reasonably well the results obtained from the experimental approaches. Interestingly, the results of U_{mf} derived from the standard deviation of cross-section averaged volume fraction measured by ECT and those obtained from standard deviation of pressure fluctuations agree very well with each other. Also, both have a discrepancy relative to the of the "benchmark" method based on pressure drop measurement within 6%.

Table 2 Summary of different approaches to obtain U_{mf}.

No.	Methods	U_{mf} [cm/s]
1	Pressure drop versus gas superficial velocity measured at six different heights	5.56
2	Standard deviation of pressure fluctuations measured at six different heights	5.23
3	Standard deviation of averaged volume fraction measured by ECT	5.25
4	Empirical correlation	4.83 – 7.19

4.2. Estimation of the minimum slugging velocity, U_{ms}

In this section, several approaches to estimate U_{ms} via pressure fluctuation and ECT measurement are discussed. The standard deviation of pressure fluctuation will be applied first. This will be followed by the analysis of pseudo 3D ECT images and standard deviation of time-resolved volume fraction of individual pixels from ECT measurement. The results obtained from these three methods will be compared to predictions from an empirical correlation.

As reviewed earlier, very few studies have been reported in the open literature where pressure fluctuation measurement would be used to predict the minimum slugging velocity, U_{ms}. **Figure 6** presents the standard deviation of pressure fluctuations measured at six axial locations as a function of the gas superficial velocity (which has a wider range than **Fig. 4**). Of course, the general trend is the same as in **Fig. 4**: after the superficial gas velocity exceeds about 5.5 cm/s corresponding to U_{mf} the pressure fluctuation level increases in an almost linear fashion with superficial gas velocity up until the highest superficial gas velocity investigated of 13 cm/s. This behaviour is understandable as the bed enters the fluidization state, first in the bubbling and then slugging regime which produce increasing flow unsteadiness.

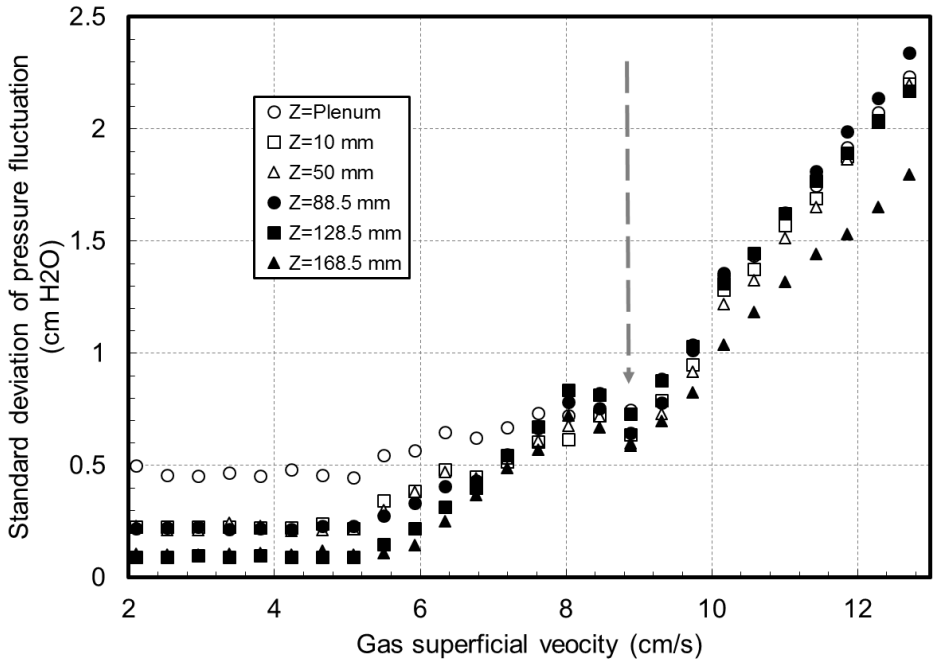

Fig. 6: Standard deviation of pressure fluctuations measured at six locations with a wider range of superficial gas velocity.

However, during this process, it can also be observed that there is an obvious "kink" in the standard deviation plot when the gas superficial velocity is at around 9 cm/s as marked by an arrow. It is hypothesised that this point could be interpreted as the onset of slugging regime, and the corresponding gas superficial velocity is the minimum slugging velocity, U_{ms} (estimated from the local minimum in the plot as 8.89 cm/s). Interestingly, Qiu et al., (2014) presented similar plots but without giving any clarification as to the nature of such "kinks". It is thought that the localised drop in the level of pressure fluctuation could stem from the change in the bubble structure. In the early bubbling regime, the bubble size increases gradually and the standard deviation of the pressure fluctuation increases accordingly. However, when the bed is approaching slugging regime, the lateral bubble growth is limited by the bed diameter, which must lead to bubble elongation and associated relative reduction in fluctuation levels. This stage is however unsustainable; a further increase in gas flow rate inevitably leads to slugging with an increased pressure fluctuation signature. These phenomena could be seen in some more detail in the pseudo 3D ECT images discussed below.

In the ECT measurement, the normalized permittivity values reconstructed from the measured capacitance values are expressed in a format of 2D, 32 x 32 matrices that form ECT images. However, if a number of such 2D image "slices" obtained for consecutive time instants in the same plane are stacked on top of one another, the pseudo-3D image can be constructed. The assumption here is of course that the flow structures passing the measurement plane are approximately "frozen" in space. **Figure 7** shows an axial cross-section of such reconstructed pseudo-3D images for the gas superficial velocity varying from 5.91 cm/s to 9.72 cm/s. The X-co-ordinate denotes relative radial position compared to the bed diameter. The Y-co-ordinate denotes time in seconds. There are 600 frames used in total, which corresponds to the time interval of 3 seconds at the ECT frame rate of 200 fps. The gas flow is from the bottom to the top. The red colour in the images corresponds to the fluidised silica sand – air mixture, while the blue colour corresponds to air. The green bands correspond to the boundaries between solids-gas mixture and air bubbles – these typically appear "fuzzy" due to the ECT image reconstruction process for a "soft" electrostatic field.

According to **Fig. 7 (a)**, the size of bubbles is fairly small compared to the bed diameter. With the increase of the gas superficial velocity (from **Fig. 7 (a) to (f)**), the size of bubbles increases gradually. At the same time, the number of bubbles increases as well (in temporal sense the frequency increases), which is evidenced by the image data presented in **Fig. 7 (e)** (14 bubbles in the image) and in **Fig. 7 (f)** (16 bubbles in the image). When the superficial gas velocity increases

further (shown in **Fig. 7 (g)**) the number of bubbles decreases slightly (to 13 bubbles). A further increase in velocity (**Fig. 7 (h)**) leads to a further reduction of the number of bubbles (11) of more substantial length, and more clear periodicity, which is a mark of transition to slugging. This is in agreement with previous findings of Liu et al. (2001), who reported that the slugging regime occurs in a seemingly periodical manner and this phenomenon can be explained well by the image in **Fig. 7 (j)**.

Clearly, the choice of the bubble boundary (the grey level of an ECT pixel) is crucial in determining the bubble size, which has been addressed in another study by Li (2016). Looking at **Fig. 7 (h)** and the bubble which appears at t=1.5 s the diameter of the bubble seems to be comparable to the bed diameter (e.g. using grey level of 0.5 as a mark of the bubble surface, corresponding to the green colour). Further increase in the gas superficial velocity leads to elongation of bubbles, without further increase in the diameter (e.g. graphs for **Figs. 7 (i) and (j)**). Therefore, it is plausible to conclude that the "kink" found in **Fig. 6** for superficial gas velocity of 8.89 cm/s marks the onset of slugging (minimum slugging velocity), which indeed is very close to 8.87 cm/s identified from the pseudo 3D ECT image analysis.

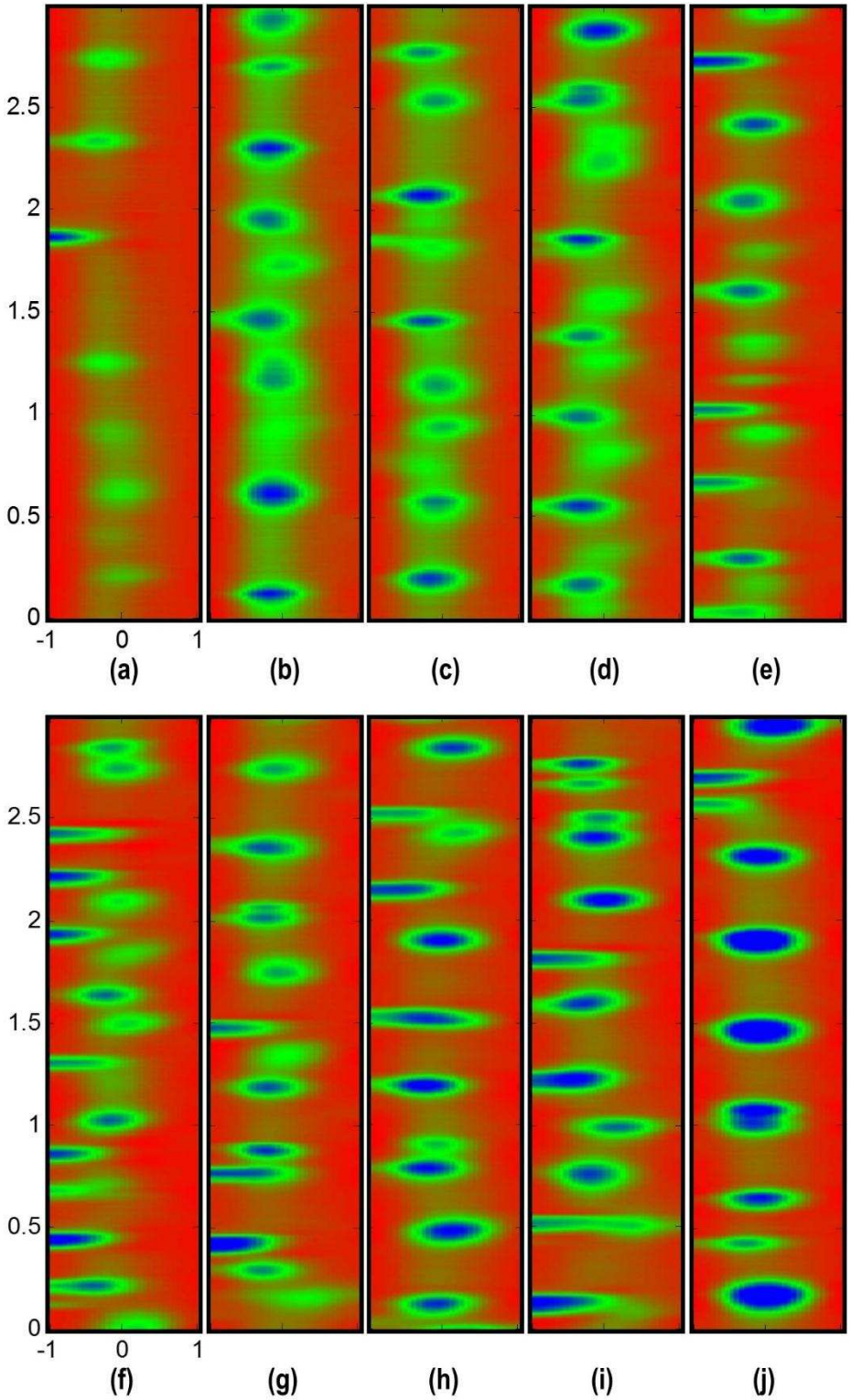

Fig. 7: Pseudo-3D ECT image analysis for various superficial gas velocities (plane 2); (a) U_0=5.91 cm/s; (b) U_0=6.34 cm/s; (c) U_0=6.76 cm/s; (d) U_0=7.18 cm/s; (e) U_0=7.61 cm/s; (f) U_0=8.03 cm/s; (g) U_0=8.45 cm/s; (h) U_0=8.87 cm/s; (i) U_0=9.30 cm/s; (j) U_0=9.72 cm/s.

In addition, it is also possible to derive the minimum slugging velocity via the analysis of standard deviation of pixel volume fraction for selected pixels in the ECT images. **Figure 8** presents the

standard deviation of volume fraction "signal" for five pixels at different relative radial positions compared to the bed radius. The selected points corresponds to the locations of the right hand "halves" of the X-co-ordinate in **Fig. 7**. With the increase of gas superficial velocity, the standard deviation of volume fraction for these five pixels steadily increases until a certain point when the superficial gas velocity is between 8.5 and 9 cm/s (as marked by a dashed arrow line). Then, the values of the standard deviation experience either a local maximum (r/R = 0.5, 0.75 and 1.0), or a change in the rate of change (r/R = 0.25). However, in the central pixel location (R=0) such change in the rate of change is hardly visible. This could be explained by the fact that the rising bubbles always take a preferable path along the centreline of the bed pipe (as seen in pseudo 3D in **Fig. 7**). It is possible that the strong fluctuation level dwarfs the finer changes in the underlying signal related to transition to slugging, which become visible for radial locations off the centreline. The U_{ms} derived by pixel volume fraction analysis is 8.87 cm/s which agrees well with the results obtained from the two approaches discussed above.

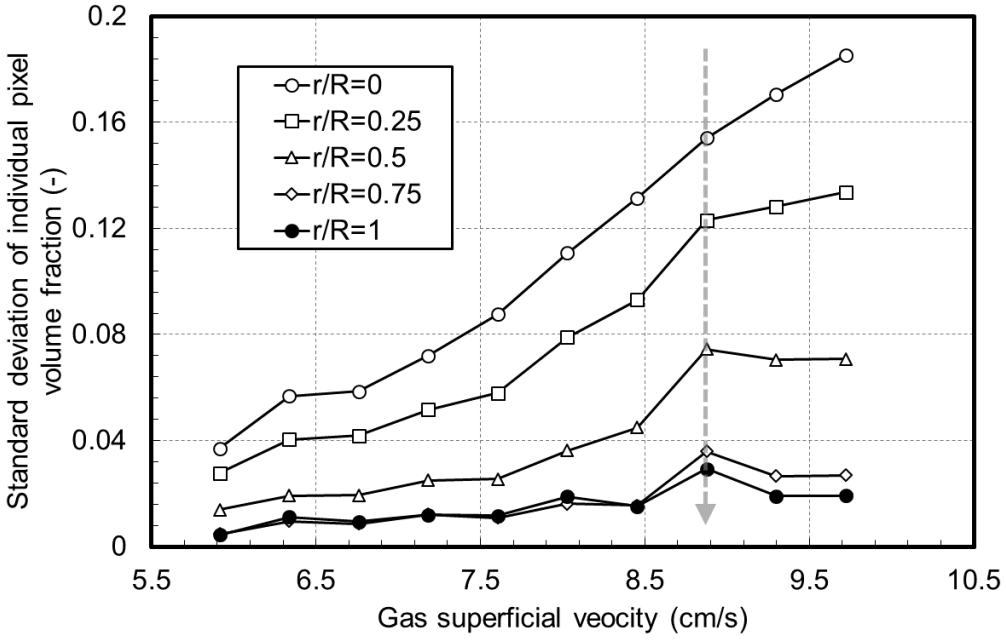

Fig. 8: Standard deviation of volume fraction "signals" for individual pixels of ECT imaging at various gas superficial velocities.

Finally, it is worth confronting the above experimental methods with the widely used empirical correlations for obtaining the minimum slugging velocity. The correlation put forward by Stewart and Davidson (1967) is often referenced as a guideline for estimating the minimum slugging velocity.

$$U_{ms} = U_{mf} + 0.07\sqrt{gD} \quad (2)$$

where U_{mf} is the minimum fluidization velocity; g is the acceleration due to gravity; and D is the diameter of the fluidized bed. As the U_{mf} was previously obtained using equation (1) with the resulting range of 4.83 – 7.19 cm/s, the resulting range for U_{ms} according to the equation (2) is 10.16 cm/s – 12.52 cm/s.

Table 3 presents a summary of the determined minimum slugging velocity using the approaches discussed in this section. The results indicate that the first three experimental approaches are in a good agreement with each other in estimating U_{ms}. Moreover, the discrepancies between the lower and upper bounds of the result from the empirical correlation and experimental results are all between 12.5% and 29.2%. It is possible that the discrepancies simply reflect the fact that the current experimental operating conditions are different from those used for deriving the original empirical correlation. Nevertheless the results from both the ECT and pressure fluctuation method show that they can be reliably used for estimating the minimum slugging velocity.

Table 3 Summary of determined U_{ms} via different approaches

No.	Methods	U_{ms} [cm/s]
1	Standard deviation of pressure fluctuations measured at six different heights	8.89
2	Pseudo-3D ECT image analysis	8.87
3	Standard deviation of individual pixel volume fraction "signals"	8.87
4	Empirical correlation	10.16 – 12.52

4.3. Dominant frequency analysis.

The PSD function is one of the most commonly used parameters in frequency domain analysis in gas-solids fluidized bed investigations. The dominant frequency derived from the PSD is effective in characterizing bubble behaviour as reviewed earlier (Qiu et al., 2014; Makkawi and Wright, 2002). Therefore, the PSD functions derived from both pressure fluctuation and ECT measurements at different gas superficial velocities will be analysed and compared. In both cases the data is obtained from two measuring locations corresponding to planes 1 and 2.

Figure 9 presents PSD functions obtained from the pressure fluctuation measurement for selected superficial gas velocities ranging from 6.76 to 12.71 cm/s. The measurements were taken using pressure port P5 (equivalent to ECT plane 2 level). It can be seen that the wide band spectra exist for two of the lowest velocities (**Fig. 9 (a) - (b)**). However, once the slugging regime is reached (**Fig. 9 (c) - (f)**), sharp (narrow band) peaks for the dominant frequencies appear in the spectra. The value of the dominant frequency increases with the increasing superficial gas velocity.

Spectra of the averaged cross-sectional volume fraction measured by the ECT are presented in **Fig. 10**. These are obtained from plane 2 for comparisons with data presented in **Fig. 9**. Clearly, **Fig. 10** also shows that broad band of power spectra appear for low superficial gas velocities. This feature usually indicates the bed in a bubbling regime with many small bubbles as explained previously (Qiu et al., 2014; Makkawi and Wright, 2002). With the increase of the superficial gas velocity, the magnitude of the power spectra also increases. Meanwhile, the broad band power spectra becomes narrow and sharp. For example, spectra for **Fig. 10 (e) and (f)** exhibit pronounced peaks for the dominant frequencies. At this stage, slugging regime dominates the bed behaviour which agrees very well with the results from pressure fluctuations shown **Fig. 9**.

The results of the investigation into characteristic frequencies using PSD analysis based on pressure fluctuation and ECT methods are summarised in **Fig. 11**. The dominant frequencies obtained from both methods agree very well in general, although some discrepancies exist for superficial gas velocities around 7.5 and 11 cm/s. The dominant frequency increases significantly at the very early stages of the bubbling regime. This is expected as more bubbles are formed to cope with increasing gas flow rate. Then the dominant frequency decreases gradually (after superficial gas velocity exceeds about 8 m/s). This may be caused by the reduction in bubble numbers due to the "merging" of the bubbles into "early" slugs during the transition into the slugging regime as it is clear that a clear drop in frequency occurs near the superficial gas velocity of around 9 cm/s. This agrees well with the discussions already provided in section 4.2 and shows that frequency analysis is also a useful tool in monitoring the state of the fluidized bed for both measurement methods presented here. Of course the observed drop in frequency in **Fig. 11** is a general trend – the more detailed inspection shows that frequency values fluctuate slightly from one velocity to another which is likely the effect of the unsteadiness in the flow regimes occurring in current experiments.

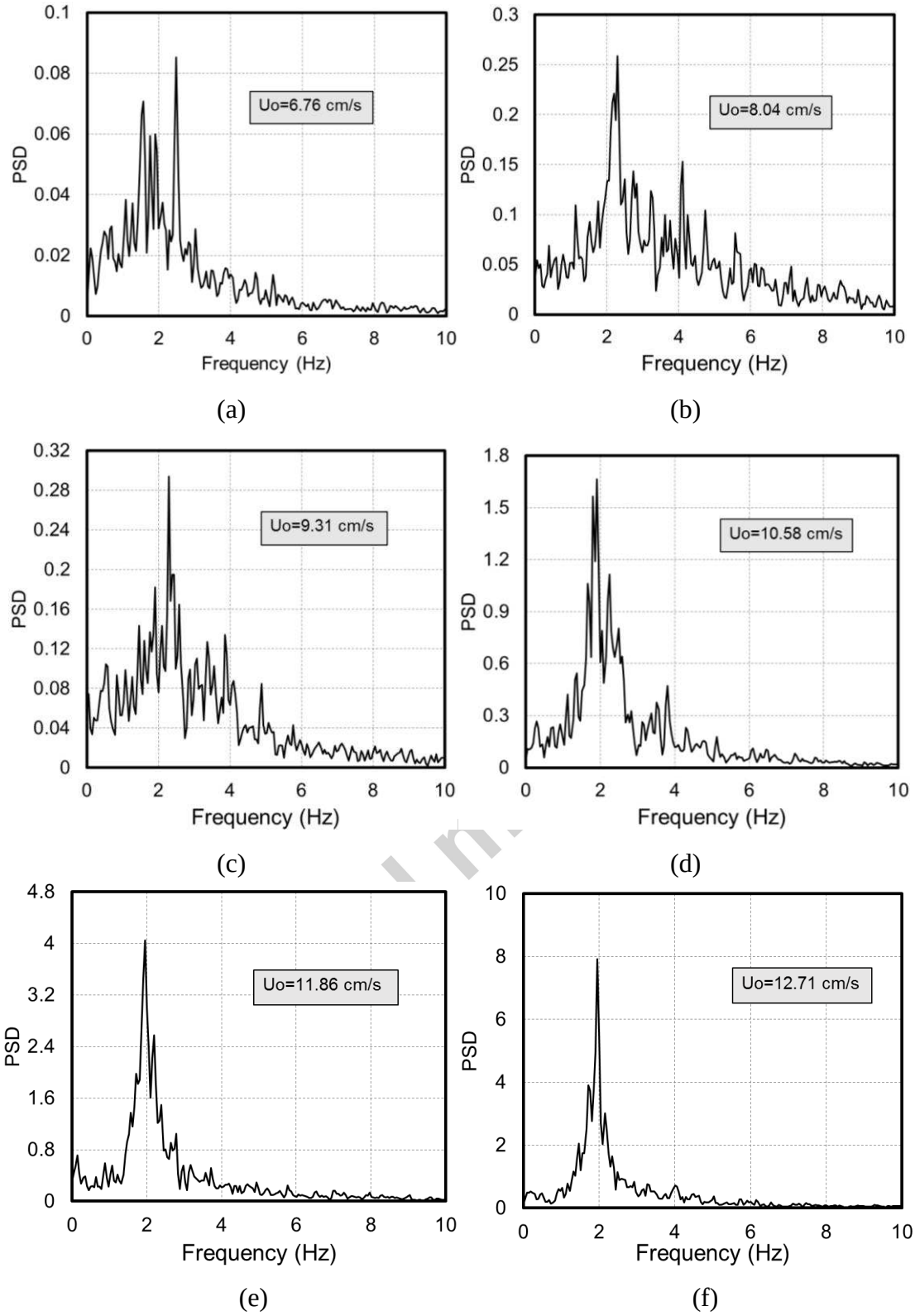

Fig. 9: Power spectral density (PSD) function obtained from pressure fluctuation measurements.

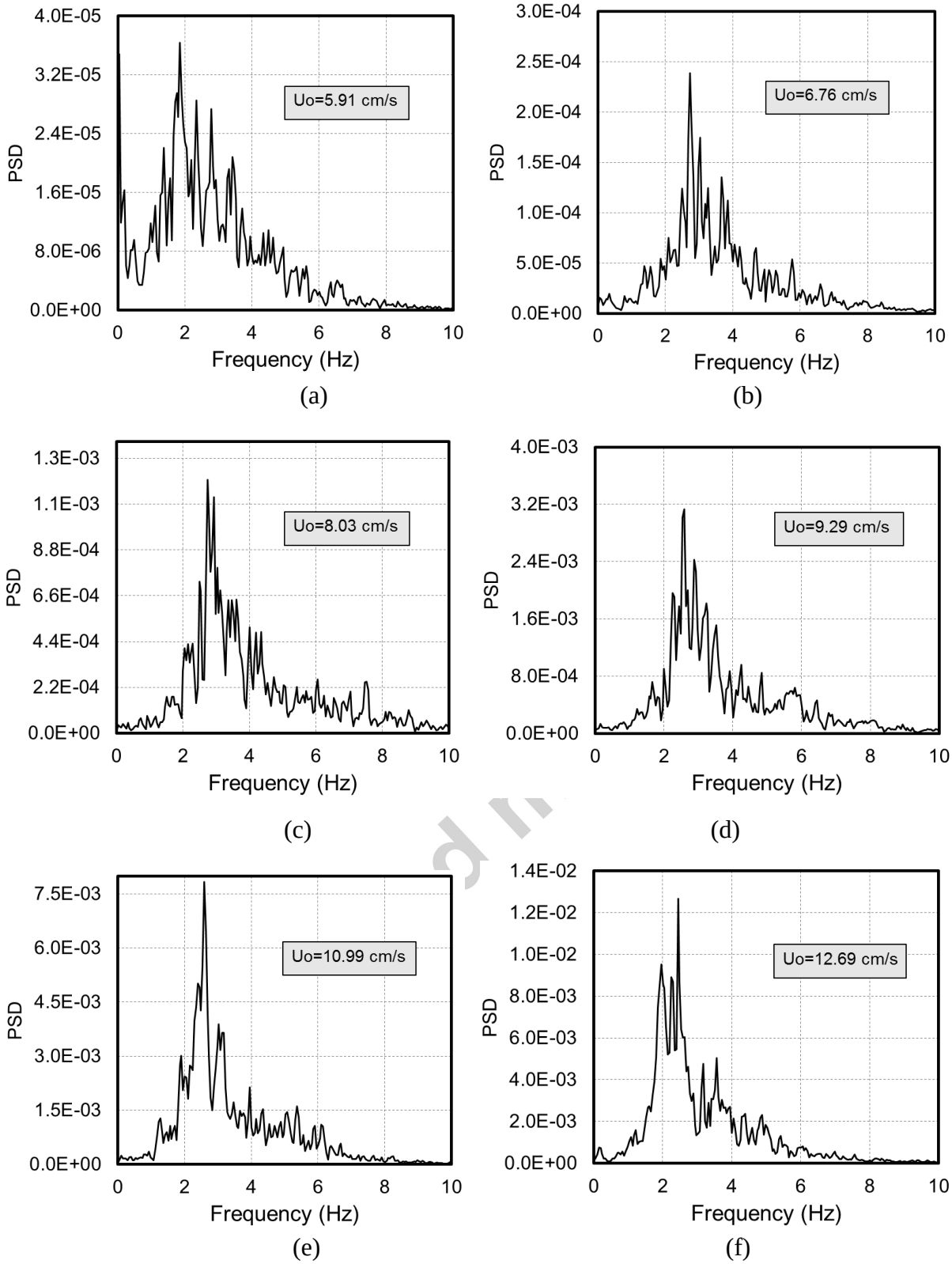

Fig. 10: Power spectral density (PSD) function obtained from ECT measurements.

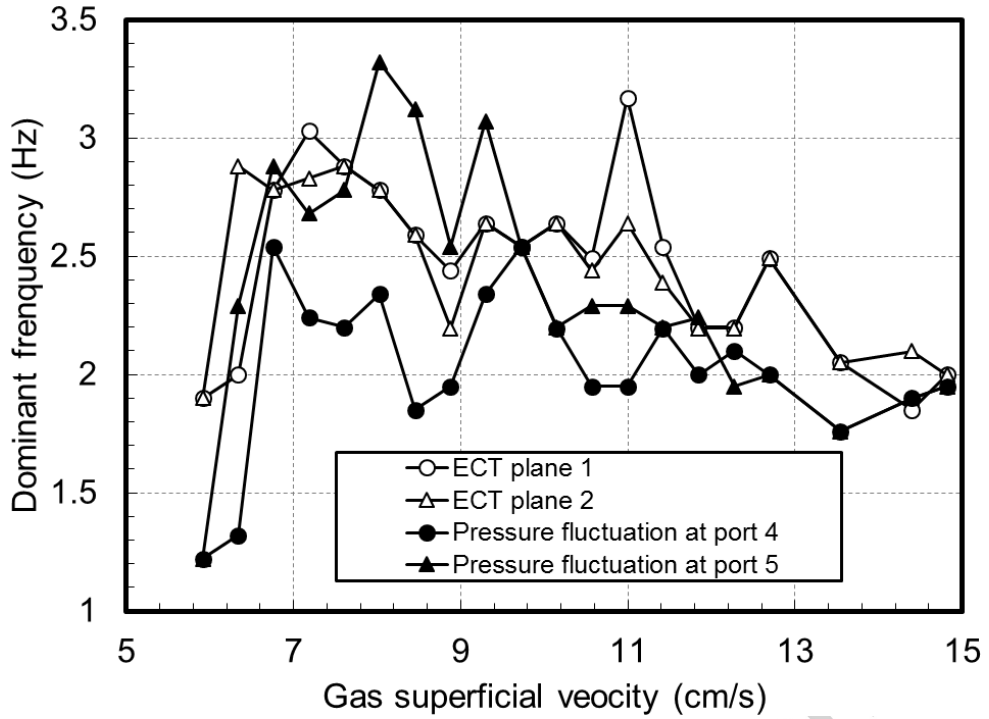

Fig. 11: Dominant frequencies obtained from pressure fluctuation and ECT analysis.

4.4. Bubble rise velocity analysis.

In general terms the bubble rise velocity is derived from measurements of time lag between two representative signals obtained from two vertical locations separated by a certain distance, and subsequently it is calculated as the ratio of the distance over time lag. The term "representative signals" is rather broad and could for example include signals from intrusive optical probes which are responsive to the presence of the passing bubbles. The interest of this paper lies in applying signals obtained from pressure fluctuations and ECT (the latter being for example cross-section-averaged or pixel-based variation in volume fraction).

An important issue in this type of analysis is also the method of obtaining the time lag values. In this paper cross-correlation techniques are used which are one of the forms of the statistical analysis of the signals obtained. The discrete format of the mathematical expression of the cross-correlation technique written after Beck and Pląskowski (1987) is as follows:

$$\hat{R}_{xy}(j\Delta t) = \frac{1}{N}\sum_{n=1}^{N} x(n)y(n+j) \qquad j = 0,1,2,\dots,J. \tag{3}$$

Here, $x(n)$ and $y(n)$ are the time series signals at upper and lower measuring locations (e.g. pressure fluctuations or ECT signals). N is the number of samples in the summation, j is the time lag between the signals of the two measuring locations and Δt is the unit time step. Clearly, the cross-correlation technique is not the only possible approach; Makkawi and Wright (2002) proposed for example so-called "detailed signal analysis" approach which relies on direct inspection of the time signals and using appropriate algebraic criteria to identify local minima corresponding to the passage of bubbles. However, cross-correlation techniques are well-established both in the general area of experimental fluid mechanics and in gas-solids flows in particular (Jaworski and Dyakowski, 2002; Dyakowski et al., 2000), and will be used here for illustration purposes.

The application of cross-correlation techniques in the context of ECT measurements will be illustrated first using the simplest case of analysing the signals obtained from cross-sectional averaging of solids concentration. **Figure 12** illustrates the normalised cross-correlation functions obtained using signals from planes 1 and 2, for a number of selected superficial gas velocities. The only difference between **Figs. 12 (a)** and **12 (b)** is the use of different scale for time lag for a better identification. The convention of the signals fed into the correlation procedure is such that the time lag is detected as negative when a disturbance is moving from plane 1 to plane 2. Also as the superficial gas velocity increases, the absolute value of time lag reduces (since the structures travel faster over the fixed distance between two planes). **Table 4** provides a summary of results obtained for different superficial gas velocities shown in the left column. Clearly, the time lag can only be estimated to the nearest "elementary time step" (second column in the table). The time step is an inverse of sampling frequency, and so for f = 200 Hz, Δt = 5 ms. Consequently, the third column contains the time lag calculated in seconds, while the fourth column contains the detected "propagation velocity" – here associated with bubble rise velocity, expressed in cm/s, and based on the separation distance between ECT planes of 40 mm. In addition, a similar analysis can be carried out using cross-correlation of signals from individual pixels denoted as (16,16) in both planes, i.e. located near the bed centreline. The resulting time lags and bubble rise velocities have been recorded in the fifth, sixth and seventh column of **Table 4**.

As can be seen from Table 4, the error of estimating the bubble rise velocity is largely dictated by the temporal resolution and is about ±5% in this study for the velocities around 30 cm/s. Obtaining a better resolution could be possible by either increasing the frame rate of ECT (in this paper the maximum was used, but faster alternative systems exist) or increasing the separation distance

between planes. The latter has of course its limitations – too large a gap may violate the usual assumptions used in the cross-correlation analysis related to existence of "frozen" flow structures that do not change significantly between sensor planes.

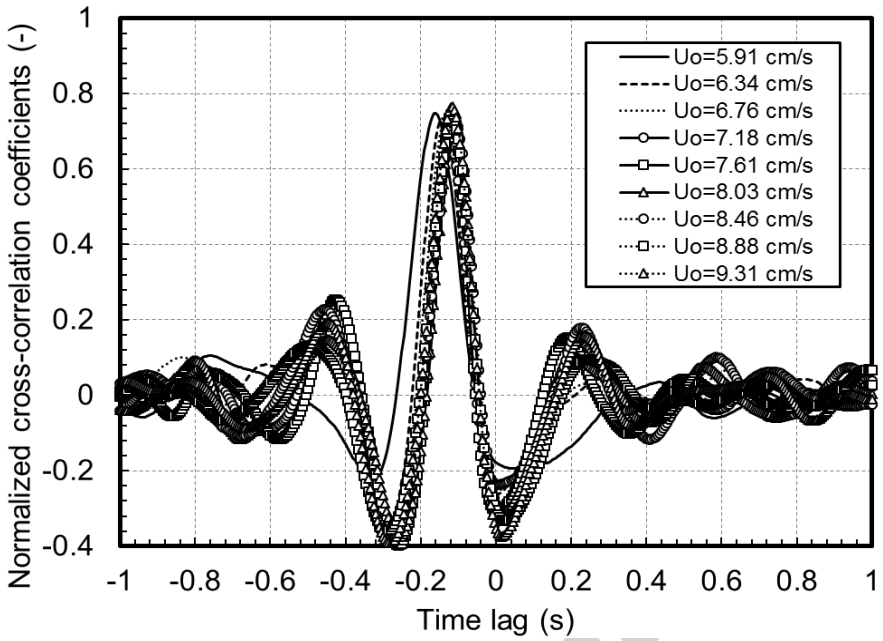

(a)

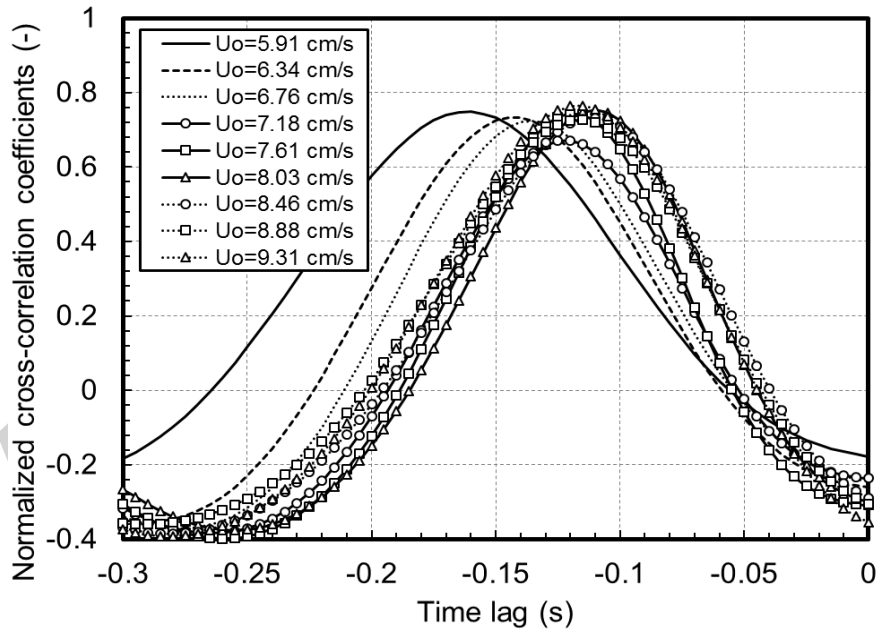

(b)

Fig. 12: Illustration of cross-correlation function vs. time lag from ECT measurements for the tested superficial gas velocities; (a) time interval from -1 to +1 s; (b) time interval from -0.3 to 0 s to show in detail the location of cross-correlation peaks.

The relatively high value of correlation coefficient for the time lags investigated (about 0.8 in **Fig. 12**) indicates that perhaps doubling the distance to 80 mm may be feasible. This has not been conducted as part of current research due to the need of designing and building an additional ECT sensor. It is also worth noting that in **Table 4** the bubble velocity seems to drop for the two highest superficial gas velocities. This is actually congruent with the discussion in section 4.2 regarding **Fig. 7** and section 4.3 with reference to **Fig. 11** where the occurrence of transition to slugging regime may cause the gas to be carried in larger "packets" that move more slowly and hence indicating a lower frequency.

Table 4 The bubble rise velocity obtained from ECT measurement based on averaged cross-sectional solids concentration signals (left) and signals from pixels 16,16 in two planes (right).

	Cross-sectional approach			Pixel-based approach		
Superficial gas velocity, (cm/s)	Time lag in elementary time steps	Time lag (s)	Bubble rise velocity (cm/s)	Time lag in elementary time steps	Time lag (s)	Bubble rise velocity (cm/s)
5.91	-32	0.160	25.00	-33	0.165	24.24
6.34	-29	0.145	27.59	-28	0.140	28.57
6.76	-27	0.135	29.63	-27	0.135	29.63
7.18	-24	0.120	33.33	-23	0.115	34.78
7.61	-24	0.120	33.33	-24	0.120	33.33
8.03	-22	0.110	36.36	-22	0.110	36.36
8.46	-22	0.110	36.36	-23	0.115	34.78
8.88	-23	0.115	34.78	-23	0.115	34.78
9.31	-23	0.115	34.78	-23	0.115	34.78

The unique capability of ECT is that it can also provide the pixel-related information, in addition to already discussed cross-section averaged solids concentration. As a simple illustration of the principle, **Fig. 13** shows the distribution of velocity over the cross-section of the bed obtained from the pixel-by-pixel correlations obtained using "signals" of local solids concentration in the corresponding pixels in planes 1 and 2, e.g. pixel k from plane 1 with pixel k from plane 2, where $k = 1, 2, \ldots, 812$. Here, the analysis is carried out for superficial gas velocity of 6.76 cm/s.

A somewhat surprising result is that the velocity profile obtained in this way is relatively flat across the cross-sectional area, even though **Fig. 7(c)** clearly shows that the bubbles are located predominantly near the centreline of the bed. It is worth emphasising again that the cross-correlation is simply a statistical tool which can detect the propagation of "disturbances" embedded in the flow process, rather than show the actual velocity values within the flow field. An interesting

question here is what kind of disturbances are being detected outside the zone occupied by the bubbles (i.e. near the bed wall). An insight to this can be obtained by carrying out a cross correlation of solid concentration "signals" from the same plane (1 or 2), but located in two different characteristic locations: here a pixel near the centre, marked as "(16,16)", is considered, together with a pixel near the wall, marked as "(16,32)".

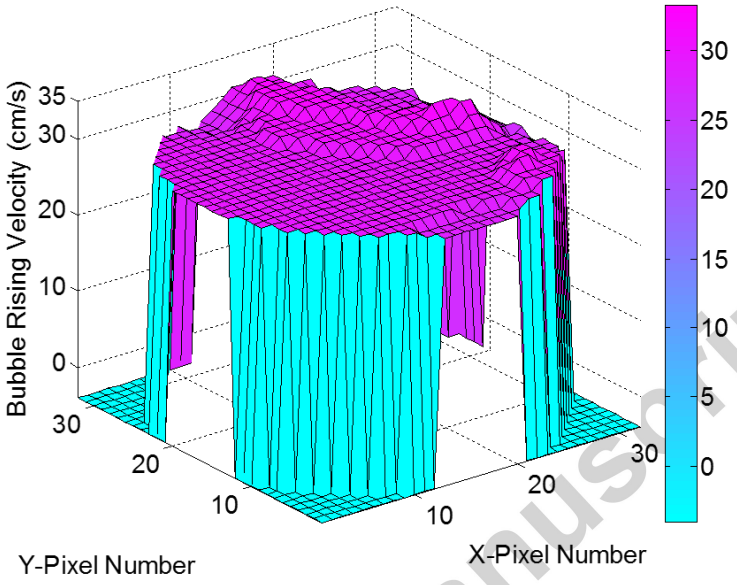

Fig. 13: Illustration of velocity distribution over the cross-sectional area obtained from "pixel-by-pixel" correlations for a selected gas superficial velocity of 6.76 cm/s.

The result of such cross-correlation analysis is shown in **Fig. 14**, where it can be clearly seen that the maximum of the cross-correlation function is at or near time lag of zero, which would indicate that the fluctuations detected in both signals are contemporaneous, but they are also in "anti-phase" indicated by the negative value of the maximum of cross-correlation (around -0.5). One possible explanation of such results is that as the bubbles pass the ECT plane the pixels near the centre detect a drop in solids concentration (bubbles tend to be empty), there is a corresponding solids "compression" on the outside of the bubbles which gives a rise in the "signal" of solids concentration in a given pixel near the wall. However, in addition, one can speculate that the cross-correlation of such pixel signals near the wall between two different planes simply detects the propagation of such "compression zones" which is simultaneous (statistically speaking) with the propagation of bubbles. Thus the propagation velocity profile in **Fig. 13** is flat.

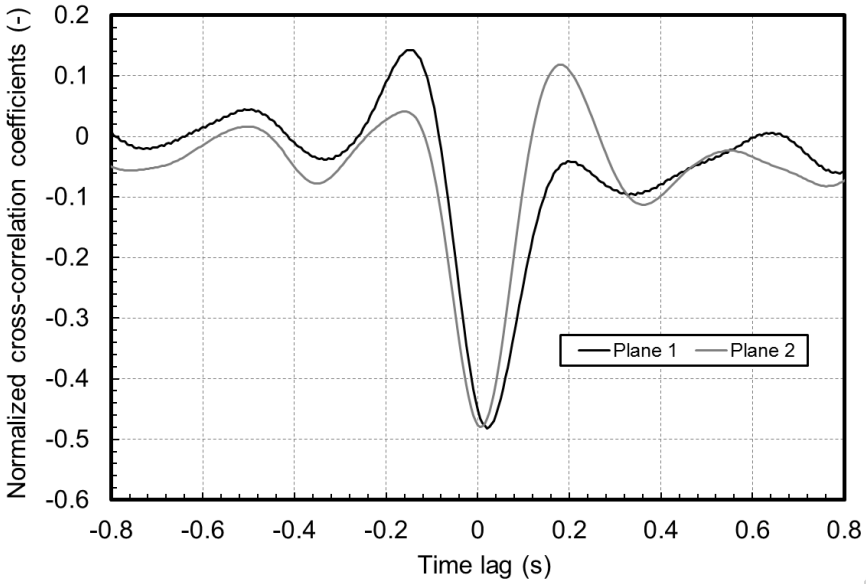

Fig. 14: Cross-correlation for pixel "signals" in the same plane: pixel (16,16) vs. (16,32) for planes 1 and 2.

The results discussed above are obviously based on the 80 second long series of ECT data, which are statistically meaningful, but may well obscure some of the flow properties that could be extracted from a more detailed analysis. As an example, it would be possible to analyse the data related to the passage of isolated bubbles (e.g. typically over the time of about 0.5 s). Clearly, such manual handling of data is time consuming and was only attempted for one row of pixels coinciding with the bed diameter – i.e. according to the previous notation pixels (16,1)…(16,32). The results of "propagation velocities" obtained this way are presented in **Fig. 15** for 11 cases of "isolated bubbles". It can be seen that in general the rise velocities of individual bubbles seen near the bed centre can vary from bubble to bubble – in this example broadly between 25 and 35 cm/s. This is expected as each bubble has a different size and hydrodynamic conditions inside the bed may be time-dependent. However, the well behaved propagation velocity profiles near the centre experience considerable fluctuations in the zone on the outside of the train of bubbles, some of the curves reaching hundreds of cm/s, which clearly falls outside of the range presented in **Fig. 15**. This may be related to the appearance of "acoustic" disturbances in the bed in addition to simple compression zones travelling with the bubble rise velocities described above. These concepts are described in more detail below in relation to pressure fluctuation measurements.

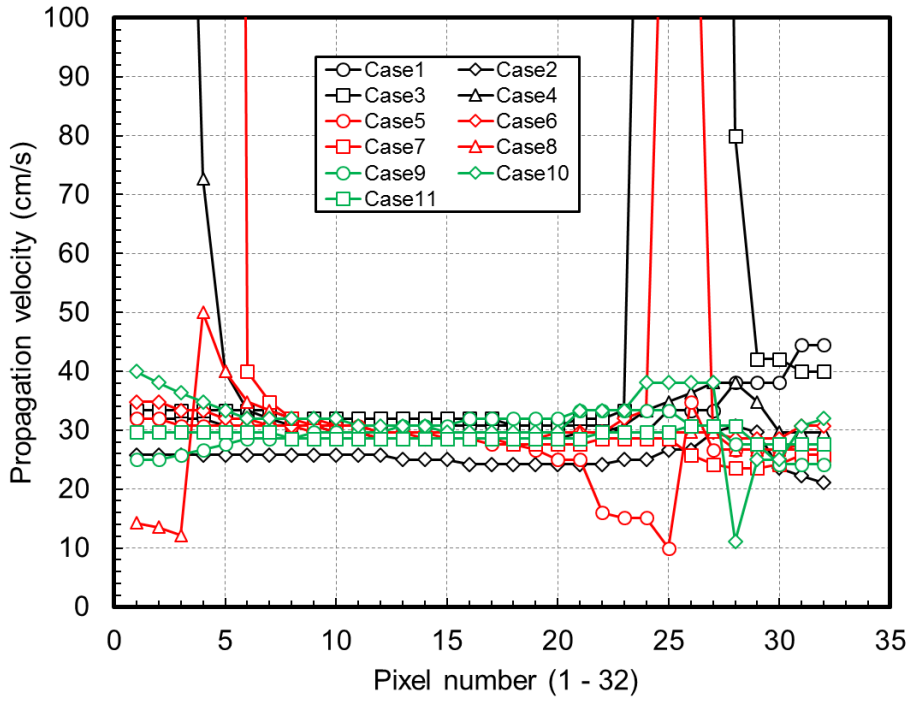

Fig. 15: Distribution of propagation velocity along selected bed diameter starting from pixel (16,1) through to pixel (16,32), obtained from cross-correlation analysis of 11 cases of isolated bubbles.

Cross-correlation analysis based on pressure fluctuation measurements is somewhat more complicated than that based on ECT. Broadly speaking, the reason for this is the inability to distinguish clearly between pressure disturbances caused by the acoustic phenomena (related to speed of sound) and the local pressure disturbances which propagate with the speed of the raising bubbles. Looking at **Fig. 16** is extremely instructive in this sense. It is split in three separate graphs, to avoid overcrowding with data, and presents the cross-correlation function as a function of time lag for selected superficial gas velocities (cf. the embedded legends), for the pressure signals obtained at locations P4 and P5 that nominally correspond to locations of planes 1 and 2 of the ECT sensor. When looking at curves in **Fig. 16 (top)** it seems that there are two competing processes at play. For the superficial gas velocities of 5.91 and 6.34 cm/s the maximum of the cross-correlation function falls near zero (small negative values of time lag), while for velocity of 6.76 cm/s the maximum appears at time lag -0.12 s. Interestingly, all three curves look as though there are underlying "double peaks", of which only one is pronounced. Further increase in superficial gas velocity, cf. **Fig. 16 (middle)**, leads to cross-correlation functions where the maxima fall into range between -0.12 s and -0.10 s although a tendency of creating a second peak at very small negative values of time lag can still be seen. Finally, in **Fig. 16 (bottom)** the cross-correlation functions change again for very high superficial gas velocities (seemingly over the slugging velocity), where

the dominant peak is again for very small negative values of time lag. It is hypothesised that this character of the correlation functions is to do with two different propagation velocities of pressure disturbances.

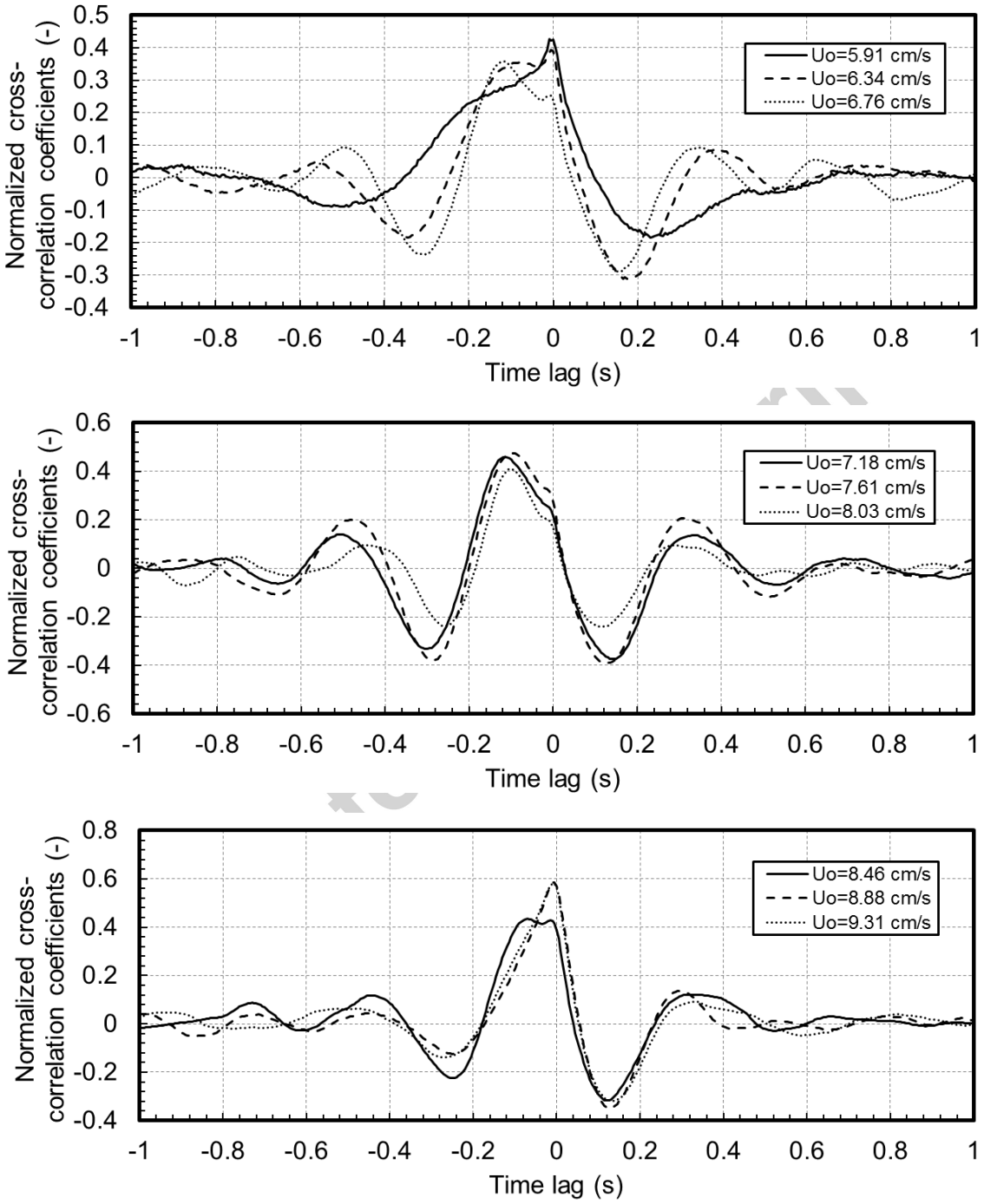

Fig. 16: Cross-correlation function vs. time lag obtained from pressure fluctuation measurements for the tested superficial gas velocities. Measurements conducted using locations P4 and P5.

It is interesting to examine previous works in the topic of velocity of sound in fluidized beds, in particular the classic paper by Roy et al. (1990). It can be found that in the gas-solids fluidized bed the speed of sound should be the speed of sound in gas times the factor: $1/\sqrt{\varrho_{solid}/\varrho_{gas}}$. Assuming the speed of sound in air at room temperature around 340 m/s, the corresponding speed of sound in the fluidized bed should be $340/\sqrt{2650/1.2} = 7.24$ m/s or 724 cm/s. **Table 5** presents the resulting velocities of "pressure disturbances" according to the applied cross-correlation analysis. Clearly, the results do not take into account the possible underlying physics, but simply base the velocities on the time lag where the maximum value of correlation function is detected.

Table 5 The bubble rise velocity obtained from pressure fluctuation measurement (using pressure transducers at locations P4 and P5). Unusable results in red.

Superficial gas velocity, (cm/s)	Time lag in elementary time steps	Time lag (s)	Bubble rise velocity, U_b (cm/s)
5.91	-1	0.005	800.00
6.34	-2	0.010	400.00
6.76	-24	0.120	33.33
7.18	-23	0.115	34.78
7.61	-20	0.100	40.00
8.03	-20	0.100	40.00
8.46	-14	0.070	57.14
8.88	-2	0.010	400.00
9.31	-2	0.010	400.00

Interestingly, the "bubble rise velocities" predicted in some cases are not physical, but seem to represent the "speed of sound" by the values in hundreds of cm/s. Please note that as the elementary time lags are only resolved down to 1 or 2 for these cases, the corresponding velocity of pressure disturbances is either 400 or 800 cm/s. On the other hand, some of the calculated bubble rise velocities seem to be in a reasonable range and close in value to the predictions from ECT. Notably values for superficial gas velocities of 6.76 and 7.18 cm/s are 33.33 and 34.78 cm/s, compared to values from ECT analysis of 29.63 and 33.33 cm/s, respectively.

Since there are actually more pressure transducer ports in the system than P4 and P5 (that correspond to plane 1 and 2), it is also possible to attempt correlations between signals of different pressure transducers. As an example two more cross-correlations have been attempted, namely P3-P5 and P3-P6. The detailed results are omitted here for brevity. However, generally similar problems as in P4-P5 correlations appear, which are related to detection of "speed of sound" instead

of bubble rise velocity in some cases. Therefore only selected cases are considered "usable" for bubble rise velocity. **Table 6** presents the results of such cross-correlation analysis.

Table 6 The bubble rise velocity obtained from pressure fluctuation measurement (using pressure transducers at locations P3&P5 and P3&P6). Unusable results in red.

	Correlation P3&P5; Distance: 7.85 cm			Correlation P3&P6; Distance: 11.85 cm		
Superficial gas velocity, (cm/s)	Time lag in elementary time steps	Time lag (s)	Bubble rise velocity (cm/s)	Time lag in elementary time steps	Time lag (s)	Bubble rise velocity (cm/s)
5.91	-2	0.010	785.00	-3	0.015	790.00
6.34	-54	0.270	29.07	-76	0.380	31.18
6.76	-2	0.010	785.00	-72	0.360	32.92
7.18	-40	0.200	39.25	-55	-0.275	43.09
7.61	-3	0.015	523.33	-39	0.195	60.77
8.03	-1	0.005	1570.00	-17	0.085	139.41
8.46	-1	0.005	1570.00	-15	0.075	158
8.88	0	0.000	∞	-6	0.030	395.00
9.31	-1	0.005	1570.00	-7	0.035	338.57

Moreover, it is possible to imagine a somewhat more involved method related to estimating the solids concentration from pressure drop measurements as introduced by Bai et al. (1996) and later revised by Liu et al. (1997). The solids concentration, δ, in the volume bounded by two pressure measurement points along the bed is expresses as follows:

$$\delta = \frac{1000\Delta H}{\rho_s \Delta L}, \tag{4}$$

where ΔH is the pressure difference between two measurement locations separated by a distance of ΔL and ρ_s is the density of silica sand. Hence, it can be hypothesised that the fluctuating values of pressure drop between ports P2 and P3 could reflect the time-dependent average solids concentration in the volume limited by these two ports. Similarly, the fluctuating values of pressure drop between ports P5 and P6 could reflect the time-dependent average solids concentration in the volume limited by these two ports. As a result, it may be useful to cross-correlate signals (P2-P3) vs. (P5-P6), in the hope that the actual cross-correlation is related to the rise of bubbles between the "volume" bounded by P2 and P3 and the "volume" bounded by P5 and P6.

Figure 17 shows the results of this cross-correlation procedure in terms of cross-correlation function as a function of time lag for nine superficial gas velocities investigated. As before, the curves are split between three graphs for the convenience of analysing the data. The correlation

functions have relatively low values (maxima reach only around 0.2) which indicates that an automated search of time lags corresponding to the maximum value of the function may not be reliable. Instead one needs to perform an informed search for maxima that correspond to the physics of the flow (rising bubbles). Results of this search are presented in **Table 7**.

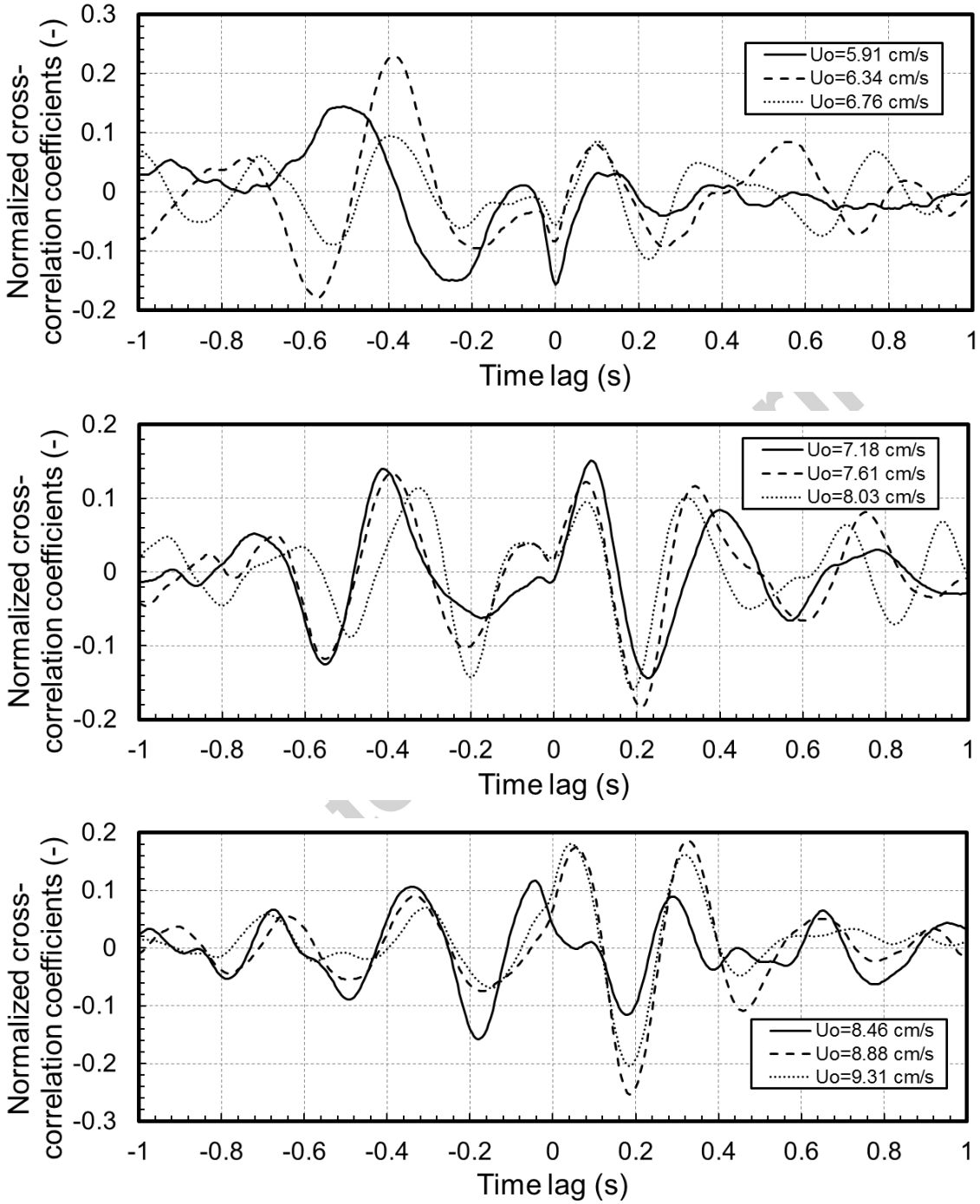

Fig. 17: Cross-correlation function vs. time lag obtained from pressure drops across P2&P3 with pressure drops across P5&P6 for the tested superficial gas velocities.

Table 7 Bubble rise velocity results based on cross-correlating time-dependent pressure drops across P2&P3 with pressure drops across P5&P6. Centre-to-centre distance is 11.85 cm.

Superficial gas velocity, (cm/s)	Time lag in elementary time steps	Time lag (s)	Bubble rise velocity, U_b (cm/s)
5.91	-101	0.505	23.47
6.34	-77	0.385	30.78
6.76	-79	0.395	30.00
7.18	-82	0.410	28.90
7.61	-78	0.390	30.38
8.03	-65	0.325	36.46
8.46	-9	0.045	263.33
8.88	-67	0.335	35.37
9.31	-61	0.305	38.85

Finally, the bubble rise velocity could be evaluated by using established empirical correlations. Two such correlations are regarded as some of the most accurate, namely those derived by Davidson and Harrison (1963) and Werther (1978), presented below:

$$U_b = U_{br} + (U - U_{mf});\ U_{br} = 0.71 \times \sqrt{g d_b}\,, \tag{4}$$

$$U_b = \varphi\sqrt{g d_b}, \tag{5}$$

where U_{br} is the rising velocity of an isolated single bubble, d_b is the bubble diameter. For Werther equation (5), the bubble diameter is obtained from his own bubble diameter empirical correlation. For Davidson equation (4), d_b is derived from popular equations proposed by Darton (1977), namely $\varphi = 0.64$ for $D \leq 10$; $\varphi = 0.254 \times D^{0.4}$ for $10 < D < 100$ and $\varphi = 1.6$ for $D \geq 100$, where D is the bed diameter with unit of cm. **Figure 18** summarises the results presented in section 4.4, together with the plots of empirical correlations calculated from Equations (4) and (5).

The results presented in **Fig. 18** demonstrate generally that the estimated bubble rise velocities based on cross-section-averaged and single pixel (16,16) data from ECT agree with each other. Davidson equation agrees with ECT for the lowest and highest values of superficial gas velocities studied, but generally under-predicts the bubble rise velocity between the two extremes. Werther equation also mostly under-predicts the bubble rise velocity except for low values of superficial gas velocities. Both types of ECT data show a slight increase in bubble rise velocities as a function of superficial gas velocity, with exception of the range coinciding with slugging, i.e. when the gas superficial velocity is beyond 8.5 cm/s, and the bed isn't strictly bubbling any more. Of course it makes no sense to plot data points based on the two correlations in the slugging regime as it is beyond their applicability range.

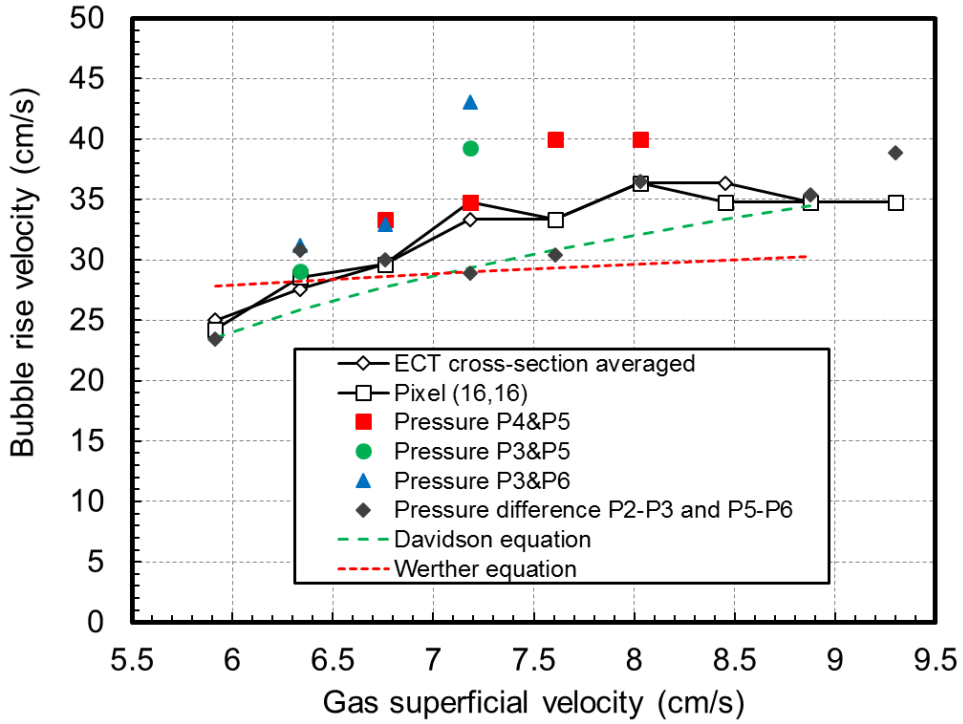

Fig. 18: Bubble rise velocity results derived by means of cross-correlation analysis using ECT (cross-section averaged and pixel-based solids concentration) and fluctuating pressure measurement. Also empirical correlations shown for comparison.

Moreover, some 'usable' points obtained from the pressure fluctuation measurement are plotted in **Fig. 18**. Interestingly, these are broadly in agreement with ECT data, especially for "pressure difference" method summarised in **Table 7** (cf. black diamonds in **Fig. 18**). However, it should be pointed out that the cross-correlation of pressure signals does not work well due to the detection of what appears to be an "acoustic speed of sound" instead of local pressure disturbances linked to flow structures. **Tables 5** and **6** illustrate the problem of invalid data very well. Further work on data processing and pre-conditioning may be needed to establish more reliable methods of estimating the bubble rise velocity using pressure fluctuation measurement.

5. Conclusions

A comparative study has been conducted to evaluate two non-intrusive measurement techniques, namely, ECT and pressure fluctuation measurement. Four parameters have been investigated and they are: the minimum fluidization velocity, minimum slugging velocity, dominant frequency and bubble rise velocity.

For the determination of U_{mf}, four different approaches were utilized. The performance of these approaches was evaluated. It has been demonstrated that the standard deviation of pressure fluctuations and ECT measurement can both effectively predict U_{mf}, in addition to the conventional pressure drop method. In terms of estimating U_{ms}, the method of using the standard deviation of pressure fluctuation measurement has been validated as being useful in combination with the analysis of ECT pseudo 3D images. In addition, the standard deviation of local pixel volume fraction have also been evaluated as being effective in determining the U_{ms} with the discrepancies between 12.5% and 29.2% compared with empirical correlation results.

Regarding the dominant frequency analysis, the comparative analysis showed that both pressure fluctuation and ECT measurements are capable of describing the bed behaviour (distinguishing the bubbling regime and slugging regime) in an effective way by analysing the width of the frequency band and the dominant frequency derived from PSD function.

It was shown that the data from either cross-sectional-averaged or pixel-based ECT measurement can be successfully used in predicting the bubble rise velocity by applying the cross-correlation techniques. Furthermore, the pixel-based local analysis with single bubble cases demonstrated the ability of the non-intrusive ECT measurement to reveal the local characteristics of bubble motion. With respect to the pressure fluctuation measurement, reasonable bubble rise velocity results can only be obtained in a limited number of cases. Additionally, it has been concluded that additional work regarding the method of deriving bubble rise velocity from pressure fluctuation measurement needs to be carried out to understand the potential limitations arising from the acoustics related phenomena.

Acknowledgments

The first author would like to acknowledge the maintenance funding from The China Scholarship Council (CSC) and tuition fees funding from the School of Civil Engineering, University of Leeds in support of his PhD programme.

References

Bai, D., Shibuya, E., Nakagawa, N. & Kato, K. 1996. Characterization of gas fluidization regimes using pressure fluctuations. Powder Technology, 87**,** 105-111.

Beck, M.S. and Pląskowski, A., 1987. Cross correlation flowmeters, their design and application. CRC Press.

Chan, I., Sishtla, C. & Knowlton, T. 1987. The effect of pressure on bubble parameters in gas-fluidized beds. Powder Technology, 53**,** 217-235.

Chandrasekera, T., Li, Y., Moody, D., Schnellmann, M., Dennis, J. & Holland, D. 2015. Measurement of bubble sizes in fluidised beds using electrical capacitance tomography. Chemical Engineering Science, 126**,** 679-687.

Darton, R.C., 1979. A bubble growth theory of fluidized bed reactors. Trans. IChemE, 57, pp.134-138.

Davidson, J.F. and D. Harrison, Fluidised particles. Vol. 3. 1963: Cambridge University Press London.

Du, B., Warsito, W. & Fan, L.-S. 2005. ECT studies of gas− solid fluidized beds of different diameters. Industrial & engineering chemistry research, 44**,** 5020-5030.

Dyakowski, T., Jeanmeure, L. F. & Jaworski, A. J. 2000. Applications of electrical tomography for gas–solids and liquid–solids flows—a review. Powder technology, 112**,** 174-192.

Fan, L., Ho, T. C. & Walawender, W. 1983. Measurements of the rise velocities of bubbles, slugs and pressure waves in a gas - solid fluidized bed using pressure fluctuation signals. AIChE Journal, 29**,** 33-39.

Geldart, D. 1973. Types of gas fluidization. Powder technology, 7**,** 285-292.

Halow, J., Fasching, G., Nicoletti, P. & Spenik, J. 1993. Observations of a fluidized bed using capacitance imaging. Chemical Engineering Science, 48**,** 643-659.

Harrison, D., Clift, R. & Davidson, J. F. 1985. Fluidization, Academic Press.

Jaworski, A. J. &Dyakowski, T. 2002. Investigations of flow instabilities within the dense phase pneumatic conveying system. Powder Technology, 125, 279-291.

Johnsson, F., Zijerveld, R., Schouten, J., Van Den Bleek, C. & Leckner, B. 2000. Characterization of fluidization regimes by time-series analysis of pressure fluctuations. International journal of multiphase flow, 26**,** 663-715.

Kage, H., Agari, M., Ogura, H. & Matsuno, Y. 2000. Frequency analysis of pressure fluctuation in fluidized bed plenum and its confidence limit for detection of various modes of fluidization. Advanced Powder Technology, 11**,** 459-475.

Li, X. 2016. Fluid Flow Processes Within Gas-solids Fluidized Beds. PhD Thesis, University of Leeds.

Li, X., Jaworski, A. & Mao, X. 2016. Investigation of bubble behaviour in a gas-solid fluidized bed by means of a twin-plane ECT sensor. 8th World Congress on Industrial Process Tomography, Iguassu Falls, Brazil.

Liu, S., Wang, S., Mason, D., Dyakowski, T. & Geldart, D. Measurement of solids concentration in gas-solid flows using capacitance tomography and pressure sensors. Proc. 8th Conf. on Sensors and their Applications, 1997. 7-10.

Liu, S., Yang, W., Wang, H., Yan, G. & Pan, Z. 2001. Flow pattern identification of fluidized beds using ECT. Journal of Thermal Science, 10**,** 176-181.

Mainland, M. E. & Welty, J. R. 1995. Use of optical probes to characterize bubble behavior in gas - solid fluidized beds. AIChE Journal, 41**,** 223-228.

Makkawi, Y. & Wright, P. 2002. Fluidization regimes in a conventional fluidized bed characterized by means of electrical capacitance tomography. Chemical Engineering Science, 57**,** 2411-2437.

Makkawi, Y. T. & Wright, P. C. 2004. Electrical capacitance tomography for conventional fluidized bed measurements—remarks on the measuring technique. Powder technology, 148**,** 142-157.

Morse, R. & Ballou, C. 1951. The uniformity of fluidization-its measurement and use. Chemical Engineering Progress, 47**,** 199-204.

Oki, K., Akehata, T. & Shirai, T. 1975. A new method for evaluating the size of moving particles with a fiber optic probe. Powder Technology, 11**,** 51-57.

Qiu, G., Ye, J., Wang, H. & Yang, W. 2014. Investigation of flow hydrodynamics and regime transition in a gas–solids fluidized bed with different riser diameters. Chemical Engineering Science, 116**,** 195-207.

Rautenbach, C., Mudde, R. F., Yang, X., Melaaen, M. C. & Halvorsen, B. 2013. A comparative study between electrical capacitance tomography and time-resolved X-ray tomography. Flow Measurement and Instrumentation, 30**,** 34-44.

Rowe, P. & Masson, H. 1980. Fluidised bed bubbles observed simultaneously by probe and by X-rays. Chemical Engineering Science, 35**,** 1443-1447.

Roy, R., Davidson, J. F. & Tuponogov, V. G. 1990. The velocity of sound in fluidised beds. Chemical Engineering Science, 45 (11), 3233-3245.

Rüdisüli, M., Schildhauer, T. J., Biollaz, S. M. & Van Ommen, J. R. 2012. Bubble characterization in a fluidized bed by means of optical probes. International Journal of Multiphase Flow, 41**,** 56-67.

Sasic, S., Leckner, B. & Johnsson, F. 2007. Characterization of fluid dynamics of fluidized beds by analysis of pressure fluctuations. Progress in energy and combustion science, 33**,** 453-496.

Stewart, P. S. B. & Davidson, J. 1967. Slug flow in fluidised beds. Powder Technology, 1**,** 61-80.

Svoboda, K. & Hartman, M. 1981. Influence of temperature on incipient fluidization of limestone, lime, coal ash, and corundum. Industrial & Engineering Chemistry Process Design and Development, 20**,** 319-326.

Process Tomography Limited. 2001. ECT User Guide. PTL300E Application Note

Van Ommen, J. R., Sasic, S., Van Der Schaaf, J., Gheorghiu, S., Johnsson, F. & Coppens, M.-O. 2011. Time-series analysis of pressure fluctuations in gas–solid fluidized beds–A review. International Journal of Multiphase Flow, 37**,** 403-428.

Wang, S. 1998. Measurement of fluidization dynamics in fluidized beds using capacitance tomography. PhD Thesis.

Wang, S., Dyakowski, T., Xie, C., Williams, R. & Beck, M. 1995. Real time capacitance imaging of bubble formation at the distributor of a fluidized bed. The Chemical Engineering Journal 56**,** 95-100.

Wen, C. & Yu, Y. 1966. A generalized method for predicting the minimum fluidization velocity. AIChE Journal, 12**,** 610-612.

Werther, J. 1974. Bubbles in gas fluidised beds -- Part II.

Werther, J., Effect of gas distributor on the hydrodynamics of gas fluidized beds. German Chemical Engineering, 1978. 1: p. 166-174.

Wilkinson, D. 1995. Determination of minimum fluidization velocity by pressure fluctuation measurement. The Canadian Journal of Chemical Engineering, 73**,** 562-565.

Yang, W.C. ed., 2003. Handbook of fluidization and fluid-particle systems. CRC press.

Highlights

- Fluidized bed flow studied by ECT and pressure fluctuation measurement methods
- Minimum fluidization/bubbling and slugging velocities from both methods compared
- Comparative study of spectral mapping and bubble rise velocity conducted
- Cross-correlation results from both methods analysed and discussed
- Acoustic propagation phenomena in the bed shown to influence the results